Effects of Nanotopography on Structural Maturation and Differentiation of Human Induced Pluripotent Stem Cell-Derived Cardiomyocytes

Winnie Wing-Yin Leung

A thesis

submitted in partial fulfillment of the

requirements for the degree of

MASTER OF SCIENCE IN BIOENGINEERING

University of Washington

2016

Committee:

Deok-Ho Kim, Chair

Jennifer Davis

Michael Regnier

Program Authorized to Offer Degree:

Department of Bioengineering

University of Washington

Abstract

Effects of Nanotopography on Structural Maturation and Differentiation of Human Induced Pluripotent Stem Cell-Derived Cardiomyocytes

Winnie Wing-Yin Leung

Chair of the Supervisory Committee:

Dr. Deok-Ho Kim

Bioengineeering

Heart diseases remain the leading cause of morbidity and mortality worldwide. As damages done to the heart are irreversible, heart transplant is the ultimate therapy, but it is greatly limited by the shortage of heart donors. Thus, scientists are attracted by induced pluripotent stem cells (iPSCs) as a solution because of their ability to be reprogrammed from a somatic cell source, potentially unlimited proliferative properties, and ability to be differentiated into many different cell types. However, hiPSC-derived cardiomyocytes display immature phenotypes in contractile properties, electrophysiology, metabolism, structure, and protein isoform expression, thus greatly limiting their application in regenerative medicine, disease modeling, and drug screening. Therefore, there is a great need for a technique to drive the

maturation of stem cell-derived cardiomyocytes to better recapitulate the properties of their adult counterpart.

Our approach was to recreate a developmentally-inspired microenvironment for maturing hiPSC-derived cardiomyocytes (hPSC-CMs). The native myocardium is characterized by aligned extracellular matrix (ECM) fibers and cells have been shown to sense and respond to cues in the ECM. In addition, thyroid hormone is a major regulator of heart development in promoting cell hypertrophy and elongation. Thus, we tested the effects of biomimetic, nanotopographical cues – using an anisotropic nanofabricated substrata (ANFS) composed of nanogrooves and nanoridges in the nanopattern (NP) – combined with thyroid hormone T3 on the structural maturation of cardiomyocytes. We found that cells exposed to nanotopography exhibited structural organization and maturation. However, the effect of T3 was not clear and appeared to have a detrimental effect at prolonged exposure at high concentration. ANFS was also used to differentiate cardiomyocytes from the cardiac progenitor stage and suggested nanotopography could have a positive effect on cardiomyocyte differentiation yield. However, experiments suggested that the differentiating cell population was highly dynamic and responded differently to the replating procedure at different time points. Therefore, a photothermal-responsive polymer was developed to introduce nanotopography with an external light stimulus, and cells were confirmed to stay attached to the polymer substrate with the topographical switch. This resulted in the development of an effective platform with vast potential, allowing the introduction of topographical cues to a cell culture with an easily manipulated external stimulus.

Acknowledgement

I would like to express my gratitude to my advisor, Deok-Ho Kim, for his guidance and supervision throughout my undergraduate and graduates years in research. Dr. Kim has given me many opportunities to learn and grow as a researcher. From all the valuable discussion with him, I have learned how to think critically and ask the right questions with a scientific mindset in research. I would also like to thank Jennifer Davis and Michael Regnier, who are on my committee and have been very resourceful and helpful in providing valuable advices to advance my thesis work.

Jesse Macadangdang, my direct mentor, has also been extremely supportive throughout my undergraduate and graduate years while working closely with me. He is always available whenever I needed help and advices, and he always pointed me to the right direction while allowing room for my independent learning and growth. Alec Smith has been very helpful and provided great insight on the development of my project. I would also like to thank Koichiro Uto for guiding me and providing his expertise in the development of the AuNR-PCL polymer, Eunpyo Choi for creation of the AuNR-PCL polymer fabrication schematics, and Peter Kim for obtaining the SEM images the AuNR-PCL polymer. TEM images were obtained from Vision Research Center Core Grant (EY01730) with the help of Edward Parker. Emil Jahng and my two undergraduate mentees Josh Katz and Sharon Ke have also helped on validating cell analysis data.

Finally, I would like to thank my family and friends. My parents have always been supportive of my decisions and always motivated me to strive and do my best. My siblings have also been there to listen whenever I needed them. Last by not least, I would also like to thank my friends who have given me so much moral support along the way. To name a few, Amy Thai,

Meena Palanisamy, and Tianwei Shen were always by my side to share my successes and failures. Ho-Tak Lau has helped me tremendously on my project by giving me suggestions during the review of my thesis material, generating the small molecule differentiation schematic, and lending me tools for the AuNR-PCL project. Jessica Wong and Kelvin Sze also provided me with much moral support during the toughest times of the project and pulling late nights with me. Ho-Tak, Jessica, and Kelvin have also given me suggestions on and helped me rehearse my oral defense presentation, as well as delivering food to me during late working hours. Without all their moral support and caring, I would not be able to come this far.

Table of Contents

Chapter 1: Introduction

1.1 Significance and Clinical Need

Heart diseases including myocardial infarction and genetic cardiomyopathies remain the leading cause of death worldwide. The only true therapeutic treatment is a heart transplant as damages done to the heart is irreversible. However, heart transplants are limited by a shortage of donors. On the other hand, using animal models for drug screening might not be a good evaluation to test drugs designed to act on human targets, making the results difficult to be translated to human [1]. Getting reliable animal systems to model different patient populations also poses a challenge. To address these issues, much effort has been devoted to human stem cell-based cardiac tissue engineering research for heart regeneration, heart disease modeling, and cardiotoxicity drug screening.

Since the discovery of induced pluripotent stem cells (iPSCs) by Yamanaka through reprogramming techniques [2], iPSCs have become a very attractive cell source in research because they can be isolated from patients in a minimally invasive fashion without ethical concerns, as with urine-derived iPSCs (UCs) [3] that are used in this thesis's studies. Like embryonic stem cells (ESCs), iPSCs are self-renewing, proliferative, and have the ability to be differentiated into any type of cells. In addition, iPSCs are patient-specific; in other words, iPSCs can be administrated back to the same host without immune response and can recapitulate the disease phenotypes from the host after their isolation and reprogramming from somatic source for disease modeling [4]. Furthermore, patient-derived hiPSC-cardiomyocytes (hiPSC-CMs) are an attractive platform to model the differences in cardiotoxicity susceptible to patients of different genetic background [5], especially because they express human ion channels similar to

primary human CMs and can be cultured indefinitely in the hiPSC form. This is especially relevant as cardiac toxicity is the leading cause of drug attrition in preclinical development, with drug-induced arrhythmia being the most common cause of drug withdrawal from the market, contributing heavily to the 1 million reported cases of adverse drug reactions [6]. Thus, hiPSC-CMs can serve as a reliable platform to screen out cardiotoxic drugs early on.

However, a major shortcoming of stem cell technology is that CMs differentiated from ESCs or iPSCs exhibit immature phenotypes in structures, electrophysiology, and functions [7]. Yet, all of the above-mentioned applications rely on CMs' ability to recapitulate the properties of their adult counterparts. For example, in order to use hiPSC-CMs for implantation to treat a necrotic area from myocardial infarction, mature phenotypes of cardiomyocytes are required for them to integrate and contract correctly and efficiently with the host to improve the function of the diseased heart. One can imagine that administrating cardiomyocytes with immature electrophysiology might cause unintentional arrhythmia in the patient when the administered cells cannot integrate correctly with host cells. Mature cardiomyocytes also allow for more accurate disease modeling of the specific disease phenotypes and more accurate drug response. Thus, it is of great importance to achieve both efficient differentiation and maturation of cardiomyocytes, which is the focus of this thesis work.

1.2 Background

1.2.1 Extracellular Matrix Modulation of Cell Fate

Before studying the effect of nanotopographical cues on the differentiation and maturation of cardiomyocytes, an understanding of the interaction between cells and their extracellular matrix (ECM) must precede. A large body of literature supports that modulation of stem cell fate and activity can be influenced by transmission of ECM biochemical and

biophysical cues to the cells [8], such as through ECM topography on the nanoscale [9], ECM biomechanical properties (i.e. stiffness, strain, cytoskeletal tension, etc.) [10], and ECM biochemical factors (i.e. growth factors and cytokines) [8]. The ECM is mainly composed of three major structure proteins: collagen, fibronectin, and laminin, as well as a concert of other proteins such as elastin, fibrillin, tenascin, glycosaminoglycan, and proteoglycans [11]. The specific composition, distribution, and assembly pattern of these proteins all contribute to the development processes as cells can sense and respond to the surrounding ECM in a dynamic manner. For example, fibronectin regulates cell migration during gastrulation just as stem cell fate is determined and the body plan and axis is being established in amphibians [12].

Meanwhile, literature has suggested that cell shape is a modulator of stem cell lineage commitment. As cells are differentiating, they undergo drastic changes in morphology; osteogenic cells become flattened as they begin to calcify matrix, while chondrogenic and adipogenic cells take on a round shape during early differentiation, and myogenic cells elongate into spindles for their muscular functions [13]. Studies have shown that changes in cell shape can regulate the differentiation of mesenchymal progenitor cells between osteogenic (adhered, flattened, and spread cells) or adipogenic (unspread and round cells) fates [10], with spread cells correlated with increased RhoA and Rho-assisted protein kinase (ROCK) activity. The effect of cell shape on osteogenic and adipogenic lineage commitment is well established. Little is known, however, about its effect on myogenic lineage commitment except that activation of Rho activity favors myogenesis and reduced Rho activity favors adiopogenesis [14]. As mentioned previously, integrin mechanotransduction from interaction with the ECM can trigger signaling cascades, including Rho family small GTPases that can in turn both regulate and be regulated by cell shape

through the modulation of the cytoskeleton, which can in turn affect cell lineage commitment through gene regulation [15, 16].

1.2.2 Extracellular Matrix Modulation of Cell Structure

Besides cell lineage commitment, RhoA/ROCK pathway has also been shown to regulate focal adhesion formation as well as maturation and actin cytoskeleton organization of cells on microtopography. Nano- or micro-topography have been shown to enhance cell adhesion strength [17, 18]. Apart from nanotopographical cues, cells are also able to sense and respond to the stiffness of the substrate. For example, Jacot et al. demonstrated that extracellular stiffness near that of the native myocardium significantly enhanced the maturation of neonatal rat ventricular myocyte with more sarcomere definition and contractile force generation [19]. Thus, it can be hypothesized that ECM cues would have an effect on cell shape and in turn myogenic lineage commitment as well as cytoskeletal organization toward structural maturation.

1.3 Current State-of-the-Art

1.3.1 Differentiation of Cardiomyocytes

Current methods to differentiate human pluripotent stem cells to cardiomyocytes include embryoid body (EB)-based and monolayer-based methods. In EB-based methods, ESCs are cultured in suspension to promote aggregation and formation of EBs before being plated down onto culture dishes [7], albeit with low efficiency of less than 1% cardiomyocytes. It was found that induction with combinations of activin A, bone morphogenetic protein 4 (BMP4), basic fibroblast growth factor (bFGF), vascular endothelial growth factor (VEGF), and the Wnt inhibitor DKK1 were able to enhance cardiomyocyte differentiation in EBs to 30-45% efficiency [20]. On the other hand, a study showed pretreatment of hPSCs with glycogen synthase kinase 3

(GSK3) inhibitors, which in effect activate Wnt/β-catenin, followed by chemical inhibitors of Wnt signaling produced a high yield of cardiomyocytes of up to 98% [21, 22], which support the temporal role of Wnt signaling has on the regulation of cardiomyocyte differentiation.

Alternatively, monolayer-based protocols have been developed for the directed differentiation of PSCs into cardiomyocytes. In general, monolayer-based protocols involve harvesting undifferentiated stem cell colonies and replating them at a confluent monolayer for differentiation induction with growth factors and/or small molecules. One protocol, the matrix sandwich method, utilizes TGFβ superfamily growth factors (Activin A and BMP4) on PSC cells that are grown on and overlay with Matrigel (MG), an ECM preparation, yielding a high purity of up to 98% cardiomyocytes [23]. Study has also found that Activin A and BMP4 have a role in inducing canonical Wnt ligand expression to affect efficiency of cardiogenesis [24]. However, it has been observed that Activin A/BMP4 directed differentiation protocol is not always successful, and differentiation efficiency is variable across cell lines [24]. In addition to the growth factor-based method, small molecule differentiation protocols have also been developed. Under the small molecule protocol, hPSCs are initially treated with GSK3 inhibitor (such as CHIR99021), followed by doxycycline-inducible expression of β-catenin shRNA (using genetic modification to express β-catenin shRNA) or IWP treatment (using small molecule inhibiting Wnt signaling), which have been shown to yield 80 – 98 % cardiomyocytes across six hPSC cell lines [25].

Overall, various differentiation protocols have been developed overtime with improving efficiency of cardiomyocyte yield, although results can be variable across different cell lines and different rounds. These protocols have employed a mainly biochemical approach to induce cardiac differentiation with the use of growth factors and/or small molecules to modulate Wnt

signaling. As nanotopographical cues have been shown to enhanced organization and structural maturation of cardiomyocytes, of interest of this thesis would be to investigate whether these cues can be incorporated earlier during the differentiation of cardiomyocytes and have beneficial effects on differentiation.

1.3.2 Maturation of Cardiomyocytes

The state-of-the-art in the field to promote cardiomyocyte maturation is based on the mechanism behind how cells interact with their surroundings. As mentioned briefly before, it is suggested that cells' peripheral proteins, such as integrins, cadherines, and non-muscle myosin II play a pivotal role in sensing other cells and the properties of the ECM such as elasticity, porosity, and topography. In response, cells conform to the microenvironment by modulating intracellular mechanics [26], such as reorganizing cytoskeletal architecture and inducing changes in transcriptional regulation [10, 27]. Thus, ECM stimuli can play a role in the maturation of cells. Mature cardiomyocytes are characterized by physiological hypertrophy, increased capacitance and cell size, elongated anistropic shapes, more organized sarcomeric structure, increased sarcomeric length, T-tubule appearance, polyploidy, greater force generation, and higher expression of genes encoding ion transport proteins and calcium handling [28-35]. Previous techniques to enhance cardiomyocytes maturation (both morphologically and functionally) include long-term culture [36]; manipulation of the biomechanical microenvironment subjecting cells to a range of stiffness [19], 3D culture environment [37], phasic mechanical stretch [38], electrical stimulation, and manipulation of biochemical cues through a number of different cytokines and growth factors [39].

Long-term culture is known to promote both morphological and functional maturation of stem cell-derived cardiomyocytes [40]. hPSC-CM cultured for 120 days show increases in cell

size, anisotropy, sarcomere length, multinucleation, calcium release and reuptake, and action potential amplitudes [36], all of which signify enhanced maturation. Another study found that after a year in culture, human induced-pluripotent-stem-cell derived cardiomyocytes (hiPSC-CMs) showed sarcomeric structural maturation with the appearance of an M-band [41]. Even though long-term culture can promote maturation, the length of time required is prohibitive due to practical and translational reasons. Thus, methods that could expedite the maturation process would enhance the utility of hPSC-CMs.

One such approach is the manipulation of the mechanical microenvironment. Jacot et al. demonstrated that cardiomyocytes grown on collagen-coated polyacrylamide gels with stiffness similar to native myocardium (around 10 kPa) promoted their functional maturation with enhanced contractile force, calcium transient properties, and SERCA2a expression [19]. However, this experiment used a flat substrate that does not fully recapitulate the geometry of the native ECM. Thus, current approaches are engineering 3D cardiac tissue structures using vascularized, porous polymeric scaffolds [42-44], scaffold-free methods [45, 46], and different hydrogels [37, 47-50]. These 3D cardiac tissue patches were shown to have better alignment, higher contractile forces, and increased maturation, as well as better translational applicability in therapy, drug screening, and disease modeling. More mechanical stimulations include phasic mechanical stretch of cardiomyocytes encapsulated in ring-shaped hydrogels [51] as well as electrical stimulation applied to cells cultured on microgrooves [52, 53] and "biowires" in collagen gel around a template suture [54]. Electrically-stimulated cells were shown to have increased maturation of contractile apparatus, better alignment and coupling, increased action potential duration, and enhanced electrical functionality. However, these studies required a more complicated fabrication process, and the design confined the orientation of electrodes in applying

an electrical field [52]. Electrodes might also create toxic by-products and have cytotoxic effect over long-term stimulation. Overall, the above attempts resulted in cell cultures of a more accurate and mature cell state than those grown on traditional flat substrates, suggesting the major role of a biomimetic mechanical environment in promoting cardiomyocyte maturation. However, these methods were not implemented in this study because they are more prohibitive for high-throughput screening and introduce higher variability to the system.

Finally, biochemical cues can also be manipulated to enhance the maturation of cardiomyocytes. A number of different cytokines and growth factors have been investigated including the administration of adrenergic receptor agonists such as norepinephrine and phenylephrine to induce hypertrophy [55, 56], thyroid hormone triiodothyronine to induce cardiomyocyte maturation [57-59], and insulin-like growth factor 1 to induce the maturation of cardiomyocyte metabolism [60]. However, these methods were not able to achieve the level of cardiomyocyte maturation seen in long-term studies.

In summary, there are a plethora of different techniques utilizing biomechanical, biochemical, and electrical cues to promote the maturation of cardiomyocytes. Independently although these methods enhanced cardiomyocyte maturation, the level of maturation was not to the extent achieved by long-term culture. Unfortunately, the length of time required for long-term cultures renders it a less attractive solution and hinders its translational applicability. Therefore, part of this thesis work is devoted to investigate whether using a combinatorial method (with both nanotopographical cues and biochemical cues) can synergistically enhance the maturation of cardiomyocytes to a greater extent.

1.4 Thesis outline

From the research in the field, it is evident that extracellular microenvironmental cues are crucial for cell proliferation, morphology, and cell fate, all of which play crucial roles in their function [61]. It is well understood that cells can sense and respond to the biochemical and mechanical cues in their environment dynamically [62]. Utilizing anisotropic nanofabricated substrata (ANFS), the goal of the thesis was to investigate the effect of combining nanotopographical cues together with biochemical cues in the structural maturation as well as differentiation of cardiomyocytes.

In Chapter 2, we tested the effects of combining nanotopographical cues with thyroid hormone T3 to promote the structural maturation of cardiomyocytes. Cells were differentiated and plated onto fabricated polyurethane acrylate substrates with presence of nanotopography and thyroid hormone. We demonstrated that nanotopography improved structural organization and maturation of cardiomyocytes, while effects of T3 were not clear at the concentration level tested.

In Chapter 3, we investigated the effects of nanotopography on the differentiation of cardiomyocytes using two different strategies. The first strategy involved replating the cell population under differentiation on Day 6 and 8, and the percentage of cardiomyocytes in culture was measured on Day 15 with flow cytometry. We observed signs of nanotopography improving the cardiomyocyte differentiation efficiency on Day 6 of replate; however, the differentiating cell population is highly dynamic and responded to the enzymatic digestion during replating very differently. Thus, in strategy 2, we developed the fabrication procedure of a photothermal-responsive polymer and demonstrated that a light stimulus could be used to induce topography change to introduce nanotopographical cues. Cells were also confirmed to stay attached upon the light irradiation and topographical change of the extracellular matrix.

Chapter 2: Combining Nanotopographical Cues with Thyroid Hormone on the Structural Maturation of Cardiomyocytes

2.1 Introduction

As previously mentioned, nanotopographical cues have been shown to promote the focal adhesion and sarcomeric organization of neonatal rat ventricular myocytes [62]. Furthermore, research has shown that Tri-iodo-L-thyronine (T3), a thyroid hormone, is a driver for hiPSC-CM maturation [59]. Yang et al. found that after 1 week of T3 treatment at 20 ng/mL, hESC-derived cardiomyocytes exhibited an increase in cell size, longer sarcomere length, higher contractile force generation, and enhanced calcium handling properties [59]. In fact, thyroid hormone is a critical biochemical regulator of many developmental processes, including cardiac growth and development in both fetal life and postnatally [63]. The activation of prohormone, L-thyroxine (T4) to the active hormone T3 leads to stimulation of nuclear thryorid hormone receptors. The stimulation of the receptors further leads to direct transcriptional activation of a wide range of genes including the increased transcription of sarcoplasmic reticular Ca^{2+} ATPase-2 (SERCA-2), α-myosin heavy chain (α-MHC), and cardiac troponin I (cTnI). Interestingly in humans, the level of T3 spikes within a few hours of birth to levels 2- to 8-folds above those in cord blood [64]. Soon after birth, cardiomyocytes exit the cell cycle and become terminally differentiated. Postnatally, serum T3 level of around 2 ng/mL remains and activates genes involved in cardiac contractility and are associated with physiological-type of cardiac hypertrophy [63].

Therefore, we focused in this chapter on investigating the effect of T3 in combination with nanotopographical cues on the structural maturation of cardiomyocytes. Although the structural maturation doesn't translate to the functional and metabolic maturation of cardiomyocytes, studying structure is definitely the first step because structure and function are

closely linked. Here, cardiomyocytes were differentiated from iPSCs reprogrammed from urine-derived cells (UCs), which were chosen for their clinical applicability, accessibility, and high reprogramming efficiency [65]. Differentiated cardiomyocyte cultures were purified through lactate selection and replated onto patterned flat and nanopatterned polyurethane acrylate substrates for two and three weeks with half of the cell population receiving T3 treatment. At the end of the second and third week, cells were harvested and measured for cell area, anisotropic ratio, sarcomeric length, and F-actin alignment. It was hypothesized that combining nanotopographical cues with T3 would promote the structural maturation of cardiomyocytes with synergistic effects.

2.2 Materials and Methods

2.2.1 Cell Differentiation

To induce cardiac differentiation, a protocol combining growth factors and small molecules (including BMP4, Activin A, CHIR99021, and Xav939) called ABCX was used [66, 67]. Undifferentiated UC3-4 colonies were maintained daily in mTeSR1 media and harvested with Versene for monolayer set-up at 250,000 cells/cm^2 on Day -2. On Day -1 when the cell monolayer reached 80-90% confluency, cells were fed with mTeSR1 supplemented CHIR99021 (1 μM) (Sigma-Aldrich). On Day 0, the confluent monolayers were induced in RPMI 1640 (Life Technologies) basal medium supplemented with B27 without insulin (RPMI/B27/Ins-) (Invitrogen) and Activin A (100 ng/ml) (R&D systems), and they were incubated in 37 °C, 5 % CO_2 for 18 hr. On Day 1, cells were kept in the RPMI/B27/Ins-, BMP4 (5ng/ml) (R&D systems), and Chiron 9902 (1 μM) for 48hr at 37°C, 5% CO_2. On Day 3 of differentiation, the media was replaced with RPMI/B27/Ins- media supplemented with Xav939 (1 μM) (Tocris Bioscience). On Day 5, cells were fed with fresh RPMI/B27/Ins- media. Starting from differentiation Day 7, the

media were changed every other day and replaced with fresh RPMI/B27 media with insulin (RPMI/B27/Ins+) (Invitrogen).

2.2.2 Fabrication of Polyurethane Acrylate Pattern

From the silicon wafer with the nanopatterns composed of ridges and grooves 800 nm apart, a first generation master mold was fabricated as an intermediate step using the polymer polyurethane acrylate (PUA; 19.8 MPa) on poly(ethylene terephthalate) (PET) films. PUA were dropped onto the silicon master, covered with PET film, and rolled out to cover the whole pattern. After UV treatment ($\lambda = 365$ nm) for 50 s to polymerize the PUA, the PET film was peeled off of the silicon wafer and the pattern was transferred onto the PET film, which was then stored under the UV lamp overnight to retain the structural integrity [68].

To transfer the pattern from the PUA-PET master to the glass coverslips on which the cells will be grown, 18 mm diameter glass coverslips were prepared by a 10 min plasma treatment followed by painting on a thin layer of glass primer. After the glass primer was dried, the polymer Norland Optical Adhesives (NOA 76) was dropped (about 15µL) onto the PUA-PET master, and the glass coverslip was inverted and placed on top (glass primer side down). Pressure was applied to roll out the NOA polymer to cover the whole area of the coverslip, and a 50 s UV treatment ($\lambda = 365$ nm) was applied to polymerize the NOA. After peeling off the PUA-PET master, the pattern was transferred to the glass coverslip, which was placed overnight under the UV lamp. The coverslips were then pre-sterilized in 70% ethanol and placed into 12-well plates for plasma treatment, UV sterilization, and ECM coating.

2.2.3 Plasma Treatment, UV Sterilization, and ECM Coating

To prepare the substrates for cell culture, the substrate surfaces were made hydrophilic for ECM protein adsorption by plasma treatment for 5 min under the 100 W power setting. Next,

they were placed under the UV lamp ($\lambda = 254$ nm) in the tissue culture hood for sterilization. To promote cell adhesion, the substrates were coated with fibronectin (BD Biosciences) (50 µg/mL in DPBS) overnight at 37°C.

2.2.4 Cell Culture for Maturation and Lactate Selection

For the structural maturation experiment in Chapter 1, cells from differentiation rounds were purified with lactate selection (2% horse serum and 4mM lactate in DMEM without glucose, pyruvate, and glutamine) for 3 days starting from Day 18 without media change until Day 21. Cells were then cultured in RPMI/B27/Ins+ to recover until they were replated on Day 27 onto patterned flat and nanopattern substrates for 3 weeks. The cells were fed every other day in RPMI/B27/Ins+, with half the cells in each substrate condition also treated with the thyroid hormone Tri-iodo-L-thyronine (T3).

2.2.5 Transmission Electron Microscopy (TEM)

At 3 weeks after the cells were replated onto patterned flat and nanopattern substrates, the cells on glass coverslips were fixed in 4 % glutaraldehyde in sodium cacodylate buffer for 2 hrs at room temperature. Then, the fixed samples were washed in buffer and stained in buffered 1% osmium tetroxide for 30 min on ice. Next, the cells were washed in water and dehydrated in a graded series of ethanol. The cells were then treated by infiltration of 1:1 ethanol: Epon-Araldite epoxy resin and two changes of pure Epon-Araldite. At this point, a second coverslip is placed on top of the cells to sandwich them in between two coverslips and for polymerization overnight in a 60°C oven. The next day, coverslips were dissolved using hydrofluoric acid, and the cells were cut out and mounted onto dummy blocks for sectioning. The sections were then used to image the intracellular sarcomeric structures of the cells.

2.2.6 Immunostaining

At 3 weeks after replate, cells were washed with PBS and fixed in 4 % paraformaldehyde and kept in PBS + 5 % FBS solution until staining. Cells were permeabilized with DPBS (Invitrogen) containing 0.1 % Triton X-100 and blocked in 5 % goat serum (Life Sciences). Primary antibody staining for sarcomeric z-discs from mouse against α-actinin (1:1000) (Sigma-Aldrich) was incubated with cells in 4°C overnight. In the following day, secondary antibodies Alexafluor 594 conjugated phalloidin (1:200) (for staining actin filaments) and Alexafluor 488 goat anti-mouse IgG (1:200) (Life Technologies) in blocking solution were incubated with cells in the dark. Finally, nuclei were stained with mounting media with DAPI (Vectashield) before imaging with confocal laser scanning microscope.

2.2.7 Data Analysis

Images were analyzed in ImageJ for cell area, anisotropic ratio for cell elongation, sarcomeric length, and Z-band width. F-actin alignment and sarcomeric length analysis were done with Matlab scripts identifying the distribution density at different orientation angles and edge-detecting sarcomeric Z-bands to measure spacing using Fourier Transform from confocal images, respectively. For Week 2 cell area and anisotropic ratio analyses, technical replicates of at least n = 3 coverslips were used, and at least 100 cells were analyzed per condition. At least 12 confocal images were analyzed per condition for sarcomeric length and F-actin analyses. As for Week 3 analyses, biological replicates of at least n = 3 rounds were performed, and at least 90 cells were analyzed from each condition for cell area and anisotropic ratio. At least 150 sarcomeric length measurements were taken using the Matlab script and 37 images from each condition were analyzed for sarcomeric width analysis from TEM images. Statistical analysis

was performed in SigmaPlot using the One-Way ANOVA test between multiple groups and Tukey test for pairwise comparison.

2.3 Results

To test the structural maturation of cardiomyocytes, differentiated and purified cardiomyocytes were replated on approximately Day 27 of differentiation onto patterned flat and nanopatterned (NP) substrates at a single-cell density. Using the thyroid hormone as a biochemical driver for cardiac maturation, half the cells cultured on patterned flat and NP substrates were fed with media supplemented with T3. Cells were harvested at 2 weeks and 3 weeks post replate onto patterned substrates and treatment with T3 for structural analysis.

At two weeks post treatment, bright-field images of the cells were taken and the cells were subsequently fixed for immunostaining. In ImageJ, the parameters of single cells were outlined and analyzed for their cell area and anisotropic ratio (**Figure 1**). It was found that the cell area of cells grown on nanopattern with and without the addition of T3 were significantly greater (around 800 μm^2) than cells grown on flat substrate with T3 (635 μm^2). Cells grown on NP also expressed an anisotropic ratio, (a length-to-width ratio) that is significantly greater (5.3) than that of cells grown on flat (2.7). As mature cardiomyocytes are characterized by hypertrophy, increased cell size, and elongated anisotropic ratio, this suggested nanotopographical cues had an effect on structural maturation of cardiomyocytes as early as 2 weeks post introduction to NP substrate.

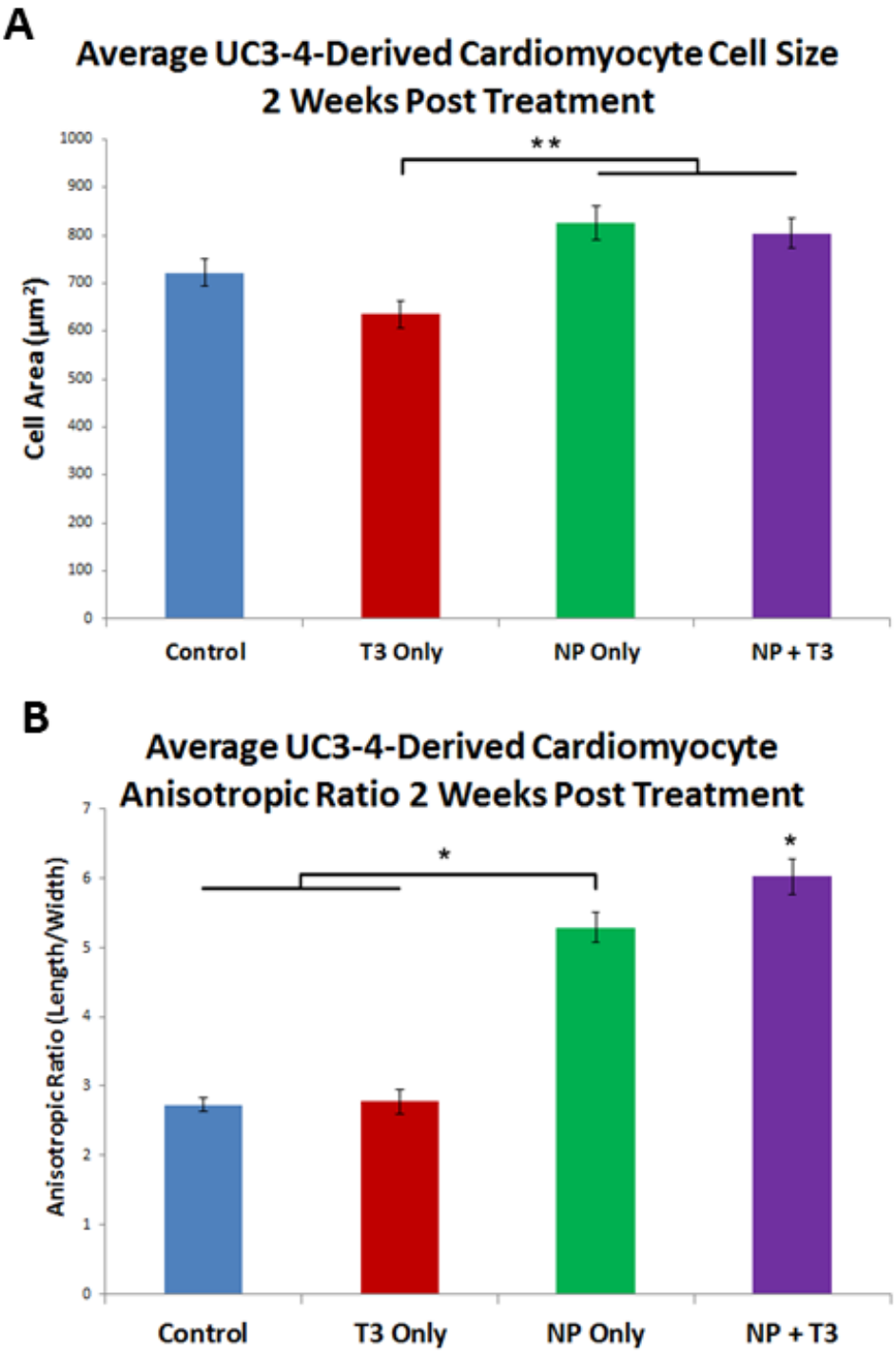

Figure 1. Cell area and anisotropic ratio of UC-derived cardiomyocytes 2 weeks post treatment. Cells grown on NP showed increased cell area (**A**) and anisotropic ratio (**B**) from cells grown on flat substrates. However, the effect of T3 on these parameters was not clear. Plotted are means ± standard errors. ** $P < 0.01$. * $P < 0.05$. P-values were calculated using one-way ANOVA and Tukey's HSD post hoc test.

Next, cells were immunostained for sarcomeric α-actinin, F-actin filaments, and cell nucleus. Confocal images were taken and analyzed using Matlab scripts for sarcomeric length and F-actin alignment measurements. **Figure 2** showed that the angle distribution of F-actin orientation filament of cells grown on nanopattern was not randomly distributed; rather, their orientation distribution has a higher distribution density at a particular angle, which is observed to be parallel to the direction of nano-ridges and nano-grooves. On the other hand, averages showed increased sarcomeric length with cells grown on nanopattern only (1.84 μm) and cells grown on nanopattern with T3 (1.87 μm) as compared to control (1.83 μm) (**Figure 3**). However, the differences between the groups were not significant. Thus, culture time on patterned substrates was increased to 3 weeks in subsequent experiments.

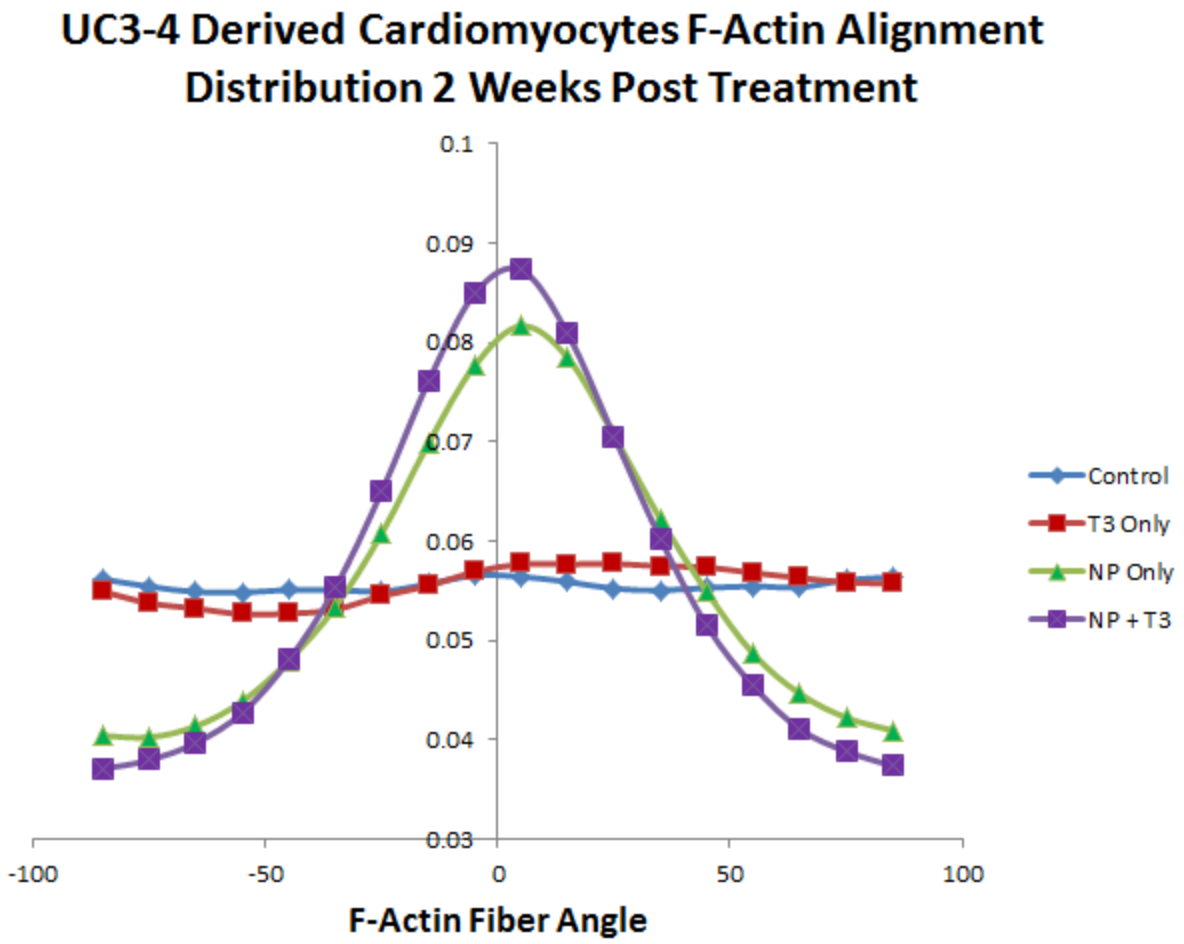

Figure 2. F-actin fiber orientation angle distribution. Cells grown on flat substrates have randomly distributed F-actin orientation angles with < 6% distribution density across all orientation angles. In contrast, F-actin fibers of cells grown on nanopattern substrates are not randomly distributed; they are shown to be aligned at a particular angle observed to be parallel to the nanogrooves and nanoridges of the NP.

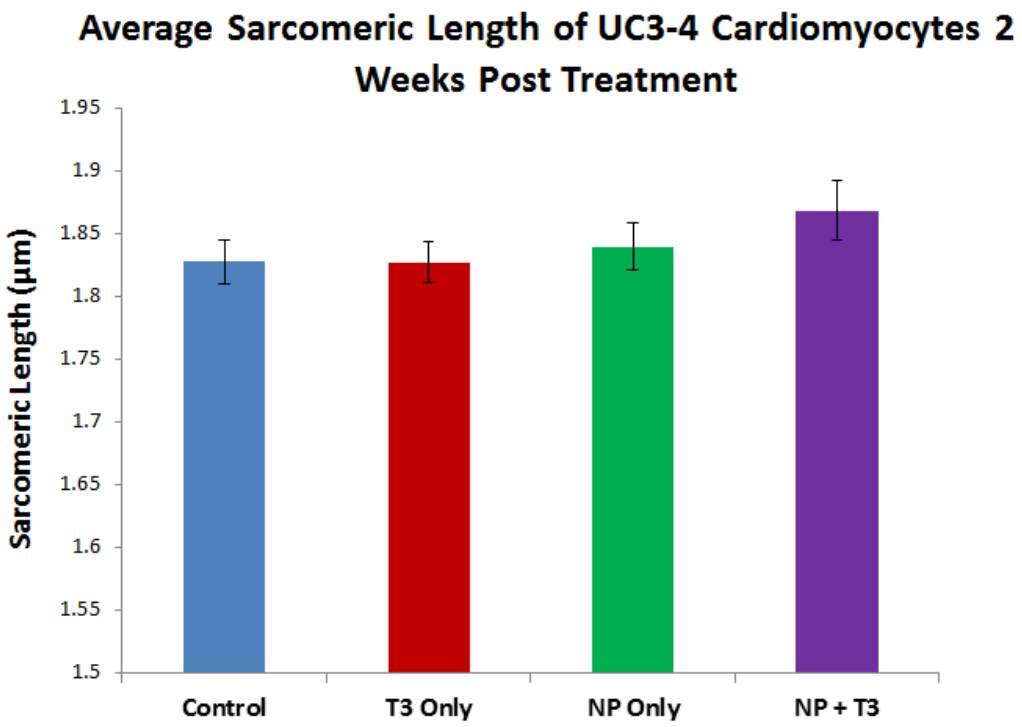

Figure 3. Sarcomeric length of UC-derived cardiomyocytes 2 weeks post treatment. The average sarcomeric length showed increase in nanopattern-only group and further increase with the addition of T3 treatment with nanopattern. However, these differences were not of statistical significance. Plotted are means ± standard errors.

Following the same procedures for the next experiment, cardiomyocytes were grown out to 3 weeks on patterned substrates with half the population getting the T3 treatment. As expected, cardiomyocytes increased in cell area when they are grown for three weeks as compared to two weeks, suggesting hypertrophy with an increase in culture time, although these were from two different experiments and no strong conclusion can be drawn between the two sets. The unexpected finding was that cells treated with T3 on flat (990 μm^2) and on NP (685 μm^2) had cell areas that were significantly lower than that of the control group (1416 μm^2) (**Figure 4**). However, the same trend at Week 3 of increased anisotropic ratios was observed in cells grown on NP.

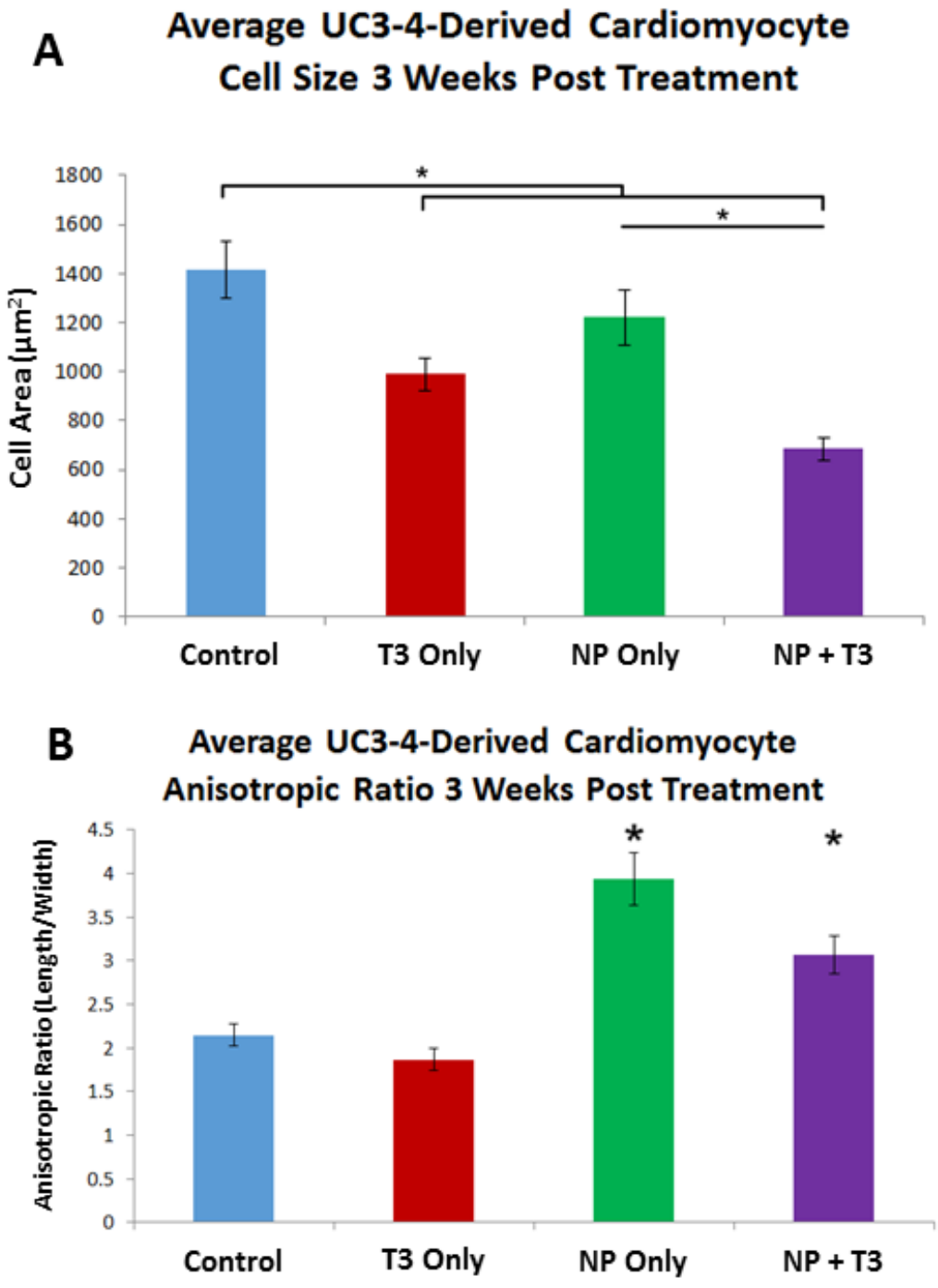

Figure 4. Cell area and anisotropic ratio of UC-derived cardiomyocytes 3 weeks post treatment. At 3 weeks after the cells were replated onto patterned substrates, cell area (**A**) and anisotropic ratios (**B**) were analyzed. Contrary to the trend from Week 2, cells at Week 3 experienced a statistically significant decrease in cell area in groups treated with T3 for those grown on Flat or NP as compared to control. However, the trend of increased anisotropic ratio in NP groups was retained at Week 3. Plotted are means ± standard errors. * $P \leq 0.05$. P-values were calculated using one-way ANOVA and Tukey's HSD post hoc test.

Next, cells were fixed to be immunostained and imaged by transmission electron microscopy (TEM). Analysis at 3 weeks showed that the control group underwent some extent of F-actin alignment, although not to the extent as those grown on NP (**Figure 5**); however, there were no F-actin alignment in the group with treatment of T3. Next, cells grown on nanopattern showed an increase in sarcomeric length of 1.67 μm (**Figure 6**), but when T3 was added with the nanotopography, the sarcomeric length (1.63 μm) was comparable to that of the control group (1.63 μm), showing no synergistic effect between T3 and nanotopography at Week 3. TEM images showed sarcomeric development with the introduction of T3 and alignment when cells were grown on NP (**Figure 7**). Specifically, cells from the control group grown on flat without T3 treatment showed underdeveloped sarcomeric structures with Z-bodies, which are fragmented Z-discs. When the cells were grown on NP, however, there were signs of M-band formation. With the addition of T3 with the nanotopographical cues, there were signs of M-bands and I-bands, which were indicative of ultrastructural organization and development of the sarcomeres.

Finally, to measure the level of myofilament bundling, the width of Z-bodies and Z-bands were measured. Figure 8 showed there were an increase in Z-band width across all treatment groups when compared to the flat, with the greatest width belonging to the group that were grown on flats with the addition of T3.

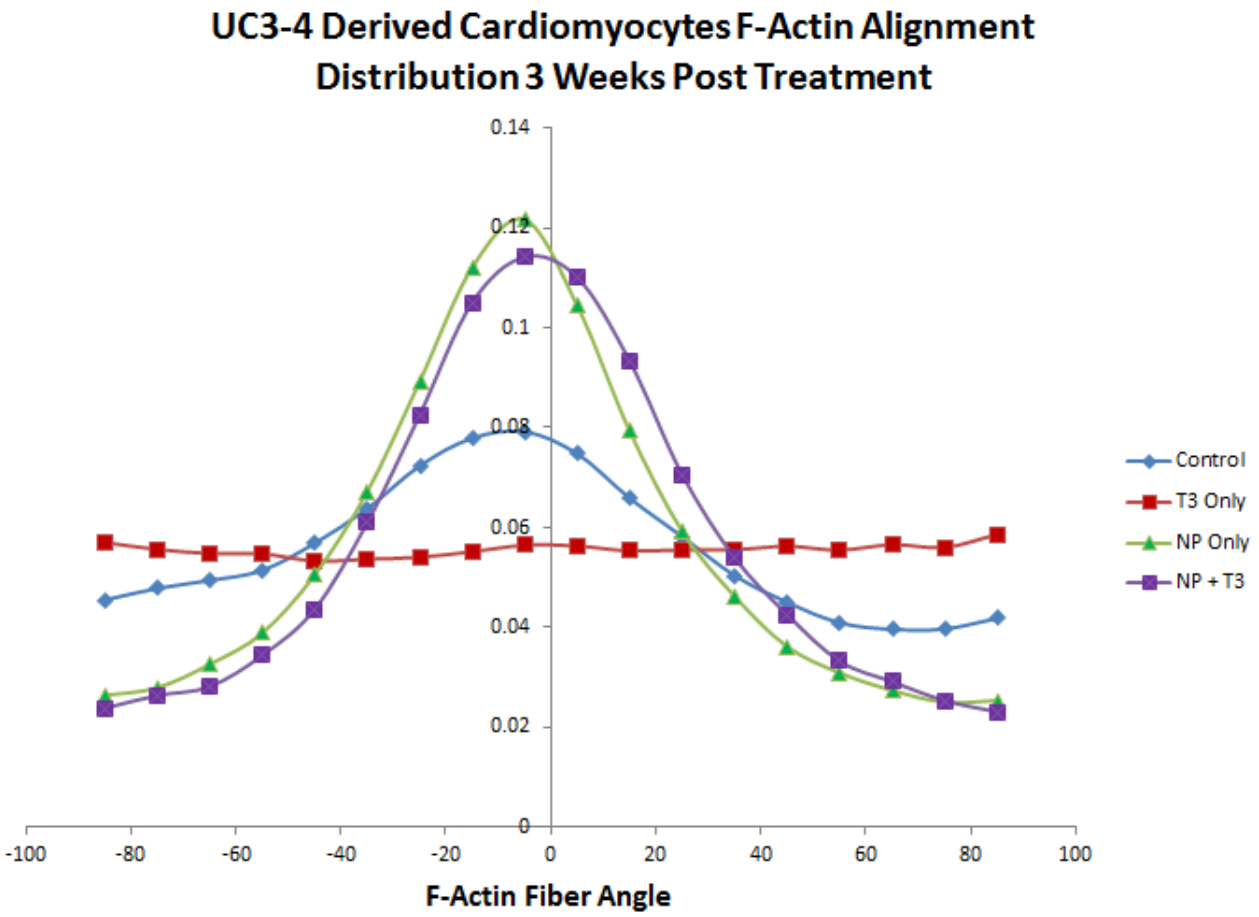

Figure 5. F-actin orientation angle distribution density of cardiomyocytes 3 weeks post treatment. Cells grown on nanopattern expressed a > 10 % distribution density at a particular angle orientation, suggesting alignment of F-actin fibers parallel to the NP. Cells grown on flat substrates have < 10 % distribution density across all orientation angles, suggesting more randomly oriented F-actin fibers from the cytoskeleton.

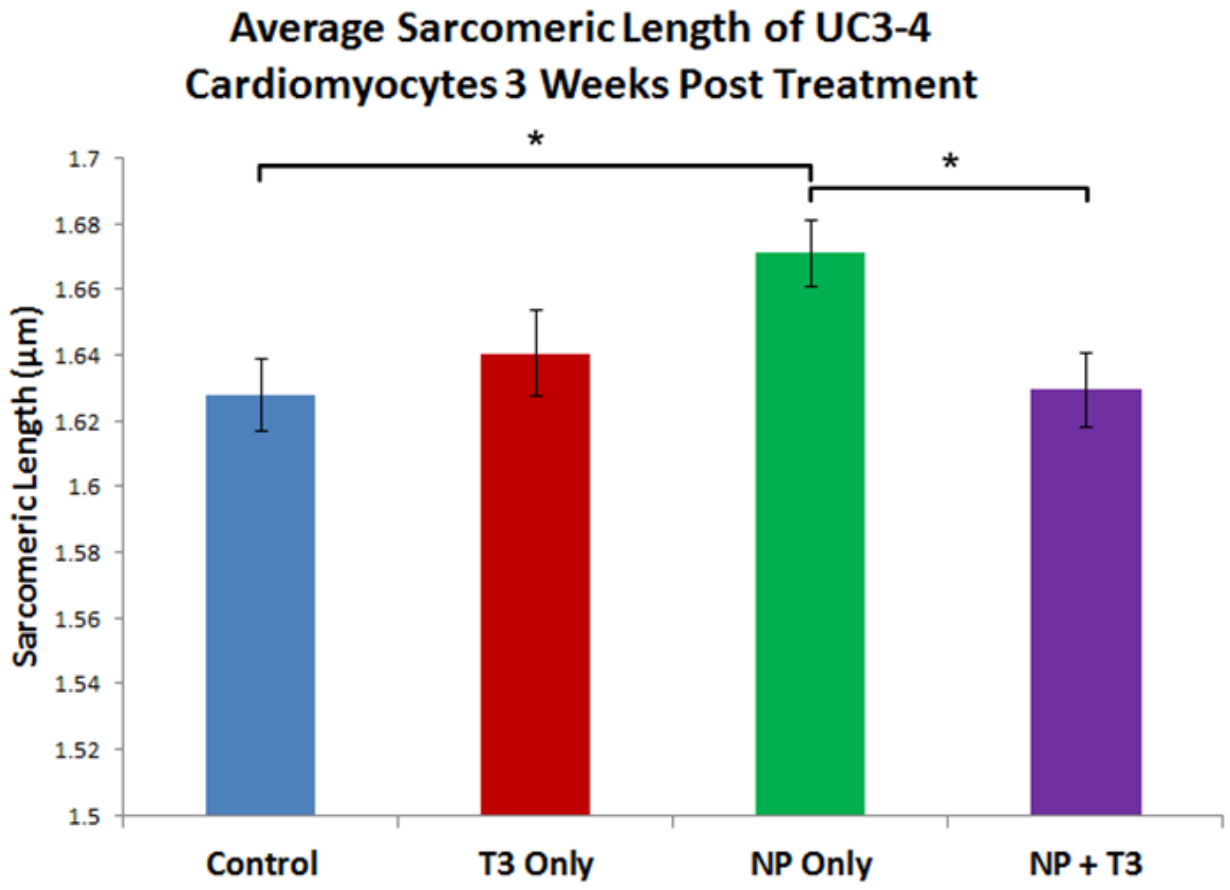

Figure 6. Average sarcomeric length of cardiomyocytes at 3 weeks post treatment. Cells grown on nanopattern only showed a statistically significant increase in sarcomeric length compared to the control group. Cells grown on nanopatterns with T3 added showed a decrease in sarcomeric length than without T3. Plotted are means ± standard errors. * $P < 0.05$. P-values were calculated using one-way ANOVA and Tukey's HSD post hoc test.

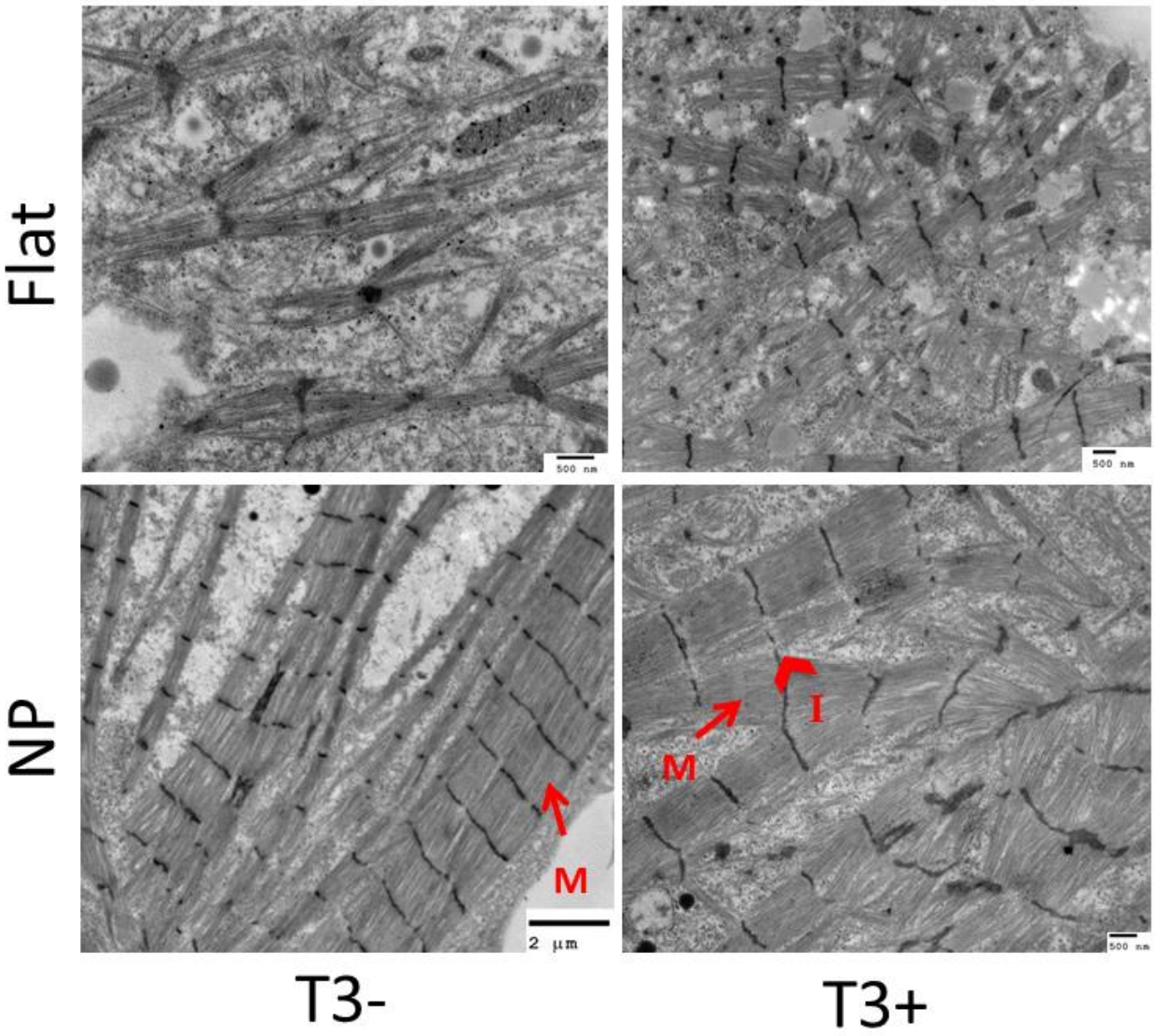

Figure 7. TEM images of cardiomyocytes at 3 weeks post treatment. Qualitatively, sarcomeres of the control group with no T3 treatment grown on flat were underdeveloped, composed mostly of fragmented Z-discs. Cells grown on NP without T3 treatment showed signs of M-bands (arrow), and cells getting the addition of T3 treatment with NP showed signs of M-bands and I-bands (arrowhead), indicative of ultrastructural organization and development of the sarcomeres.

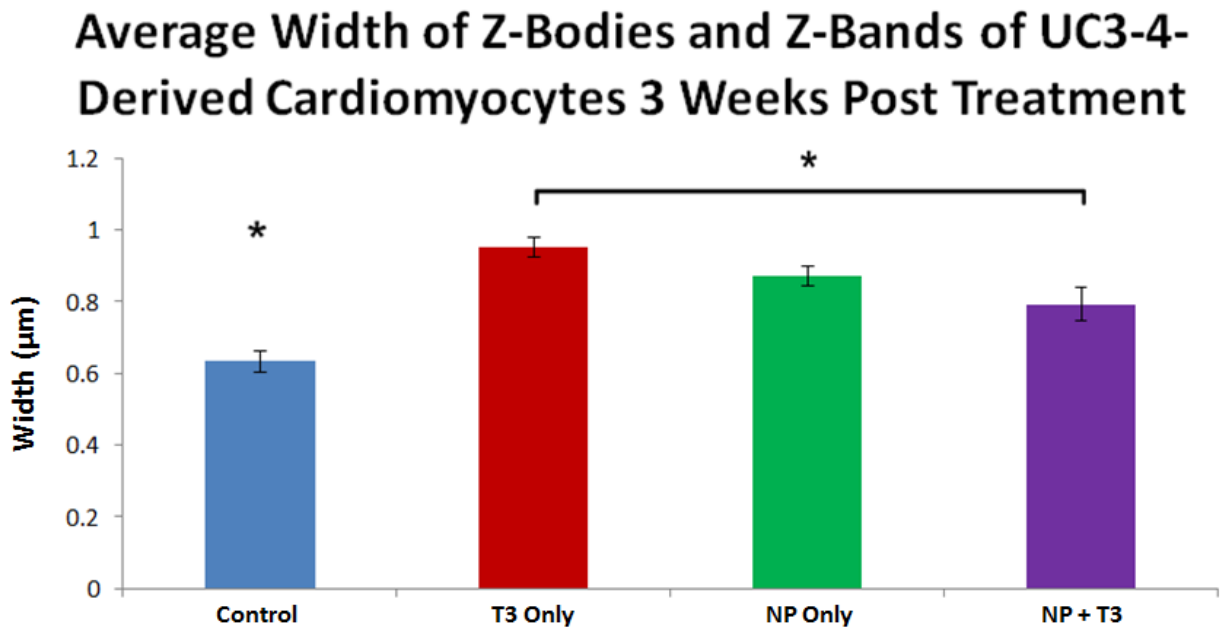

Figure 8. Z-bands and Z-bodies width of hiPSC-CMs. All treatment groups experienced a statistically significant increase in Z-band/Z-body width compared to the control, suggesting myofilament bundling. The greatest width belonged to the group with T3 treatment only grown on flat substrates. Plotted are means ± standard errors. * $P < 0.05$. P-values were calculated using one-way ANOVA and Tukey's HSD post hoc test.

2.4 Discussion

As stated in the introduction, there is a need to drive the structural maturation of hiPSC-derived cardiomyocytes to have them more closely recapitulate the phenotypes of their adult counterpart for their applicability in regenerative medicine, disease modeling, and drug screening. This chapter focused on using nanotopographical cues in conjunction with treatment of T3 to promote the structural maturation of cardiomyocytes. It was hypothesized that the combination of T3 and nanotopography would have a synergistic effect on the structural maturation of cardiomyocytes. Data showed that nanotopographical cues have a tremendous effect in structural development and organization, by aligning the cytoskeleton of cardiomyocytes (F-actin alignment), elongating the overall cell shape (increased anisotropic ratio), increasing the

sarcomeric length and Z-body/Z-band width, and showed signs of ultrastructural organization of the sarcomere with the detection of M-bands. One thing to note about the data was the sarcomeric lengths at 3 week of around slightly above 1.6 μm, which is around the length of a myosin thick filament [69] and suggested that the cells might be in systole. Although the cells were washed with DPBS without calcium before fixation in an attempt to relax the sarcomere by getting rid of calcium ions, perhaps a calcium chelator should be used to make sure calcium ions are eliminated and that the cells are under diastole during fixation for future experiments. Nonetheless, the data suggested that cells can sense and respond dynamically to the extracellular matrix, resulting in structural organization and maturation. As the cell substrates were coated with fibronectin, it is highly likely that cells sense the extracellular matrix through integrin focal adhesion complex that can bind to the RGD motif present in fibronectin, resulting in mechanotransduction and changes in cell morphology and cytoskeletal development [70-72].

Literature has suggested that thyroid hormone T3 is a major regulator of many developmental processes, playing a major role in heart development to promote hypertrophy and elongation of the cells [59, 64]. However, although the data did suggest nanotopography having an effect on structural maturation and organization in cardiomyocytes, the effect of T3 were not clear. In fact, cell area actually decreased upon the treatment with T3. This is speculated to be due to detrimental effects caused by prolonged exposure of an elevated level of thyroid hormone. In human, the level of T3 spikes within few hours of birth and subsequently drops to a constant serum level of around 2 ng/mL postnatally [63]. Yang et. al. had shown that a 1 week treatment of T3 at an elevated level of 20 ng/mL improved cardiac performance and promoted hypertrophy [59]. However, this effect does not seem to hold for prolonged treatment to 2 and 3 weeks. An *in vivo* study have also shown that administrating an elevated level of T3 for a prolonged period of

time in rats resulted in an increase in uncoupling proteins, which is associated with a decrease in mitochondrial efficiency [73]. Thus, this suggests that cardiomyocytes are sensitive to the exposure of T3 hormone both in concentration and length of time. Furthermore, results from the literature and this experiment also suggested there is an optimal concentration and exposure time of T3 to cardiomyocytes that can promote their maturation. A sign of hypertrophy emerged when cardiomyocytes were grown for 3 weeks when they were cultured for longer period of time compared to 2 weeks. At 3 weeks, the overall averages of cell area increased across the different conditions. However, the data between the two weeks were from two separate experiments and more experiments from utilizing the same differentiation cell batch is needed to confirm this difference. Thus, more studies testing different levels of T3 and exposure time to cardiomyocytes are needed to find the best treatment condition for structural maturation of cardiomyocytes.

Chapter 3: Effects of Nanotopography on Cardiac Differentiation

3.1 Introduction

Current differentiation protocols of cardiomyocytes involve a host of signaling molecules that direct the PSCs to a mesoderm and subsequently cardiac lineage that mostly act on the Wnt/β-catenin signaling pathway [74], but how biophysical cues in the form of nanotopography affect cardiomyocyte lineage commitment is poorly understood. Since cardiomyocytes have been shown to sense and respond to nanotopographical cues, a natural question would to be to ask whether these cues could be introduced at an earlier time point that could drive the differentiation of stem cells into cardiomyocyte. Cardiac progenitor cells (CPCs) can be differentiated into cardiac, smooth muscle, and endothelial cells [75], and Wnt/β-catenin inactivation is necessary for CPCs to exit the proliferative state and transition into cardiomyocytes. This is the developmental time point that we focused on to investigate the effect of introducing nanotopographical cues on the differentiation of CPCs into cardiomyocytes at the onset of Wnt/β-catenin inactivation. This is a logical time point to introduce the nanotopographical cues because from a biological standpoint, pluripotent stem cells were not exposed to cues biomimetic to those of the native myocardium, and the cues might activate undesired signaling cascade that can potentially drive the stem cells down the wrong lineage by interfering with the dominant Wnt/β-catenin signaling cascade. Thus, it was hypothesized that introducing biomimetic, nanotopographical cues at the cardiac progenitor stage would enhance the cardiomyocyte differentiation efficiency. To achieve the introduction of nanotopographical cues during the differentiation process, this chapter is broken down into the following two strategies.

Strategy 1: Introduction of nanotopography during the cardiac progenitor cell stage by replate. The differentiation of UCs into cardiomyocytes was induced on traditional tissue culture polystyrene (TCPS) plate until Day 6 and 8 when the cells are transitioning from cardiac mesoderm to CPCs and replated onto patterned substrate to carry out the rest of the differentiation – to test the efficiency of CPCs differentiation into cardiomyocyte on flat versus NP substrates. Cells were harvested on Day 15 and stained for the cardiomyocyte marker cardiac troponin T (cTnT) to gauge the success of the differentiation from flow cytometry.

Strategy 2: Fabricate and characterize a smart-material substrate capable of topographical switch from photothermal effects for use in the differentiation of cardiomyocytes. During the differentiation process from stem cells to cardiomyocytes, the cell population is highly dynamic in cell type composition and stages of lineage commitment. Furthermore, the disassociation process often breaks down the cell adhesion molecules and proteins connecting the cells to the substrate and to each other, which play a large role in the fate of these cells. Thus, there is a need for the development of a biocompatible smart-substrate that can switch from flat to nanopatterned topography with an external stimulus, negating the need to enzymatically dissociate the cells. The smart-substrate would be based on a shape memory material crosslinked from poly(ε-caprolactone) (PCL) macromonomers. The successful material would retain a temporary shape (flat) at physiological temperature of 37^{o}C and switch a permanent shape (nanopattern) at around 39 - 40^{o}C to be applicable for cell culture experiments. The topographical switch would be induced based on photothermal effects to keep the culture aseptic. With the successful development of this material, the introduction of nanotopographical cues could be manipulated easily and be controlled to allow direct comparison between different time points.

3.2 Materials and Methods

3.2.1 Cell Differentiation

With the small molecule protocol, the glycogen synthase kinase-3 inhibitor CHIR99021 and Wnt inhibitor IWP-4 were used [25]. Undifferentiated UC3-4 colonies were maintained daily in mTeSR1 media and harvested with Versene for monolayer set-up at 250,000 cells/cm^2 on Day -1. On Day 0 when the monolayer reached 100% confluency, cells were fed with mTeSR1 supplemented CHIR99021 (12 μM) (Sigma-Aldrich). At 24 hours later on Day 1, media were replaced with RPMI/B27/Ins- media until Day 3, at which the cells were fed with RPMI/B27/Ins- media with 5μM IWP-4. On Day 5, cells were fed with fresh RPMI/B27/Ins- media. Starting from differentiation Day 7, the media were changed every other day and replaced with fresh RPMI/B27 media with insulin (RPMI/B27/Ins+). Depending on the experiment, the differentiating population were replated on Day 6 or Day 8 onto patterned polyurethane acrylate coverslips in 12-well plates (fabrication method explained under "Fabrication of Polyurethane Acrylate Pattern" under Materials and Methods section in Chapter 2) to continue the rest of differentiation into cardiomyocytes.

3.2.2 Plasma Treatment, UV Sterilization, and ECM Coating

To prepare the substrates for cell culture replate, the substrate surfaces were made hydrophilic for ECM protein adsorption by plasma treatment for 5min under the 100 W power setting. Next, they were placed under the UV lamp (λ = 254 nm) in the tissue culture hood for sterilization. To promote cell adhesion, the substrates were coated with fibronectin (BD Biosciences) (50μg/mL in DPBS) or Matrigel (1:60 in DMEM) overnight at 37^{o}C for 4^{o}C, respectively.

3.2.3 Flow Cytometry

On Day 15 of differentiation, coverslips were taken out of each culture well and washed with DPBS, so only cells that were exposed to the substrate treatment were harvested. A portion of cells (at least 300,000 cells per condition) were enzymatically digested (with TrypLE Select), broken into single cell suspension, and fixed with 4% paraformaldehyde (PFA) for 10min in room temperature in the dark. Cells were then kept in PBS + 5% FBS solution until staining. For staining, cells were permeabilized in 0.75% saponin (in PBS + 5% FBS) and stained with the primary mouse IgG antibody, cardiac troponin T (cTnT) (1:100). Secondary antibody staining were performed in the dark with Alexafluor 488 goat-anti-mouse IgG (1:200) (Life Technologies) in 0.75 % saponin solution (in PBS + 5 % FBS). Finally, cells were washed in PBS + 5 % FBS solution and transferred to FACS tube for analysis of purity and differentiation efficiency, gated for the population of alive cells. Technical replicates of n = 3 coverslips from each condition were used for each set of experiment, and One-Way ANOVA test between multiple groups and Tukey test for pairwise comparison were performed to analyze differences.

3.2.4 Preparation of AuNR-PCL Solution

The gold nanorod poly(ε-caprolactone) (AuNR-PCL) solutions were prepared with 50 wt% PCL to 50 wt% organic solvent dichloromethane (DCM). Specifically, AuNR-PCL solutions were made using 80 to 20 wt% of two- and four-branched PCL (2b- and 4b-PCL) [76], respectively, with 10 wt% photo initiator (2,2-dimethyoxy-2-phenylacetophenone) mixed with 0.5, 1, or 3 wt% gold nanorods (AuNR) dissolved in (DCM). The solution is then vortexed for 2 min and sonicated for 20 min or until homogenous.

3.2.5 Fabrication of AuNR-PCL Films

A permanent shape with 1:1 nano- ridges and grooves of 800 nm dimensions were induced by crosslinking 50 - 60µL of AuNR-PCL solution on top of a 800 nm patterned PDMS master mold with Teflon spacers (1 cm^2 squares) and sandwiched between two glass slides with clamps. The top and bottom are UV cured (λ = 365 nm) for 6min on each side to ensure complete crosslinking. The films are then peeled out and washed in acetone solutions for 1hr, replacing with fresh acetone solutions every 15 min to remove un-crosslinked PCL monomers. As PCL polymer swells in acetone, the AuNR-PCL films are then placed in methanol solution for 10min to allow the polymer to return to original size. Next, the films are placed in 60^{o}C oven for at least 4hr above the melting temperature for transition to amorphous state. To deform the films to induce a temporary flat shape, the films are then clamped between two flat Teflon sheets, two PDMS blocks, and two metal plates and placed back into the 60^{o}C oven for 20 min (ensuring amorphous state) before it is placed into -20^{o}C freezer for 30min for transition to crystalline state to fix the film at the temporary, deformed shape. The films would only return back to the permanent shape at above melting temperature. The films are then pre-sterilized under UV lamp (λ = 254 nm) in the tissue culture hood for 1hr each side and placed into 24 W plates in preparation for plasma treatment, UV sterilization, and ECM coating.

3.2.6 Immunostaining

After the AuNR-PCL polymers seeded with cells received light irradiation to induce a topographical change, the polymers were immediately washed in PBS twice for 5min each time to get rid of cells that lifted off. The cells on the polymer were fixed with 4% paraformaldehyde. Cells were permeabilized with DPBS (Invitrogen) containing 0.1% Triton X-100 and blocked in 5 % goat serum (Life Sciences). Primary antibody staining for vinculin from mouse (1:1000) and

Alexafluor 488 conjugated phalloidin (1:200) (for staining actin filaments) in blocking solution was incubated overnight in 4°C. Secondary antibody Alexafluor 594 against mouse in blocking solution as incubated with cells in the dark. Finally, nuclei were stained with SlowFade® Diamond Antifade Mountant with DAPI (Life Technologies) before imaging with confocal laser scanning microscope.

3.3 Results

Strategy 1: Differentiation replate on Day 6 and 8 onto polyurethane acrylate patterned substrates.

During the differentiation of PSCs into cardiomyocytes (**Figure 9**), Wnt/β-catenin signaling activation is necessary for mesoderm formation and generation of cardiac progenitor cells [74]. Glycogen synthase kinase-3 (GSK-3) functions to phosphorylate β–catenin, targeting it for degradation. Thus, using the glycogen synthase kinase-3 (GSK-3) inhibitor, CHIR99021, would result in the accumulation of β–catenin and Wnt activation. In the next stage for cardiac progenitor cells to be terminally differentiated into cardiomyocytes, Wnt/β-catenin signaling needs to be inhibited [77], and this was done with the Wnt signaling inhibitor IWP-4. Introducing nanotopographical cues between day 5 and 8 when the cell population was transitioning from cardiac mesoderm to cardiac progenitor cells would provide cues that are biomimetic to those found in native myocardium at the correct developmental stage. Two time points (Day 6 and Day 8) were chosen to replate the differentiating cell population onto substrates with nanotopographical cues in the form of nano-ridges and nano-grooves.

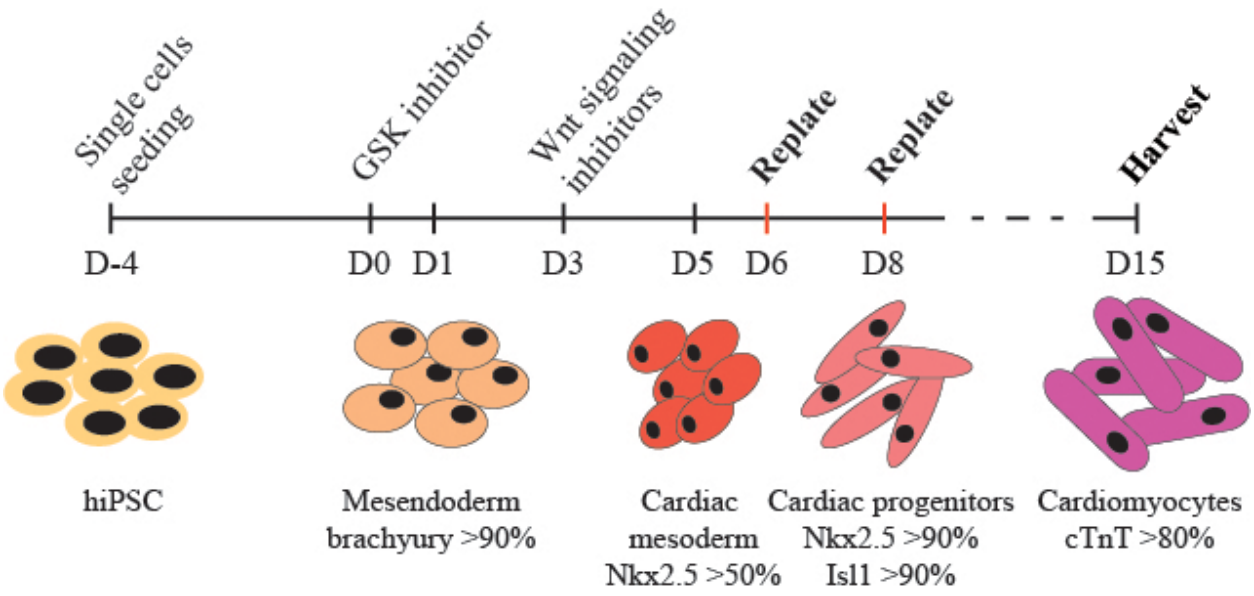

Figure 9. Small molecule differentiation of cardiomyocytes. The differentiation of iPSC into cardiomyocytes is regulated by initial Wnt signaling activation with a GSK inhibitor to promote the formation of mesendoderm and cardiac progenitor cells. Next, Wnt signaling inactivation is necessary to convert cardiac mesoderm into terminally differentiated cardiomyocytes. Cells going through the differentiation procedure were replated on Day 6 and Day 8 onto fabricated polyurethane acrylate substrates.

For the experimental set-up, UC3-4s were differentiated on TCPS using the small molecule protocol described in the Materials and Methods section before they were replated on Day 6 and 8 of differentiation (when they became cardiac progenitor cells) onto patterned substrates. To isolate the effect of the fabricated substrate on the differentiation process without masking effects from substrates such as Matrigel (which contains laminin, collagen, proteoglycans, and a number of growth factors), fibronectin was chosen as the ECM to coat the patterned substrate because of the RGD binding site for integrin receptors that promote cell adhesion [78]. A study also found that around 60 % cardiomyocyte differentiation efficiency from hPSC can be achieved on TCPS coated only with fibronectin, although the ratio giving the highest efficiency is 70 % fibronectin and 30 % laminin [79]. The experimental group was CPC

culture that were replated on Day 8 onto fibronectin coated patterned flat and nanopatterned substrates, while control substrate groups include traditional MG-coated TCPS without replate, MG-coated TCPS for replate on Day 8, MG-coated patterned flat and nanopatterned substrates, and FN-coated TCPS for replate (**Figure 10**).

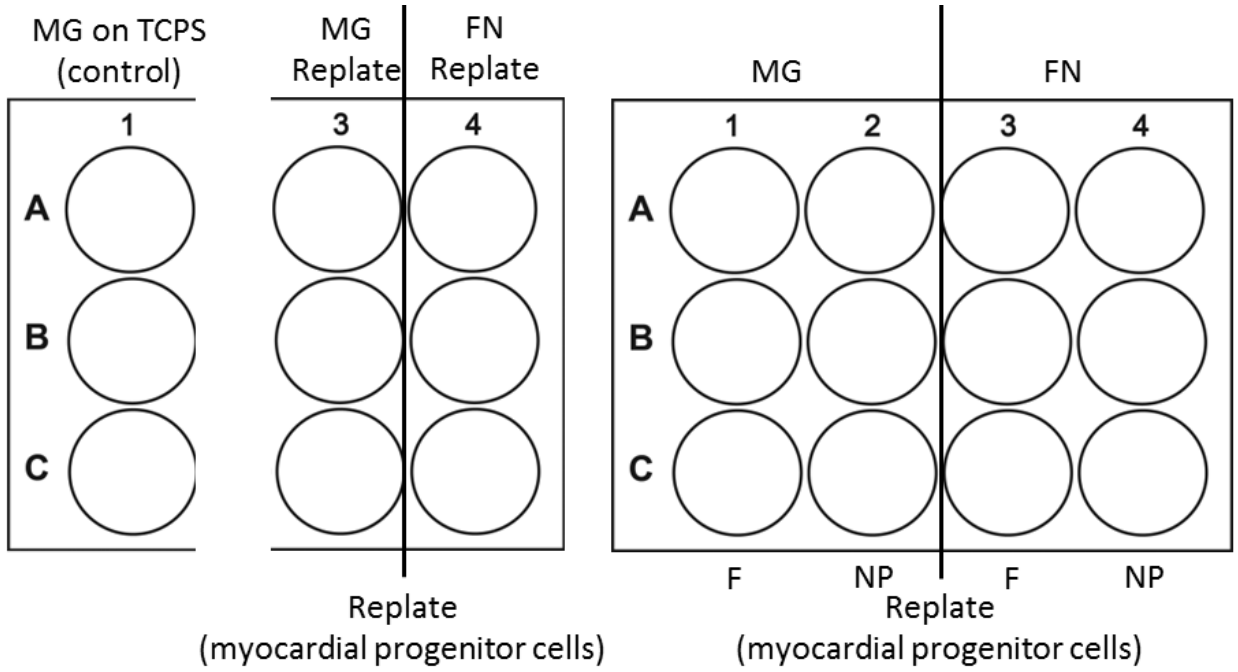

Figure 10. Experimental Set-Up. Cells were differentiated on MG-coated TCPS until either Day 6 or 8, and a subset of cells were harvested and replated onto fibronectin coated patterned flat and nanopatterned substrates (experimental groups), as well as control substrate groups including MG-coated TCPS, MG-coated patterned flat and nanopatterned substrates, and FN-coated TCPS. Each substrate condition had triplicates.

For the Day 6 replate time point from the differentiation round (images in **Figure 11**), cells were replated at a high density of 500,000 cells/cm^2 as cell-cell contact had been observed to be important during the differentiation of cardiomyocytes and for cell-cell signaling that could activate differentiation-associated genes and alter genotype and phenotype [80]. On Day 7, cells were observed to adhere to all conditions, and they were grown out to Day 15. On Day 15, cells

from all conditions exhibited beating, and cells were more confluent for the MG coated substrates as compared to the FN-coated substrates. This might be explained by pluripotent growth not promoted by fibronectin-based matrices [81]. On Day 15, dead cells were washed away with DPBS and attached cells were harvested for flow cytometry gated for the population of alive cells. Flow cytometry data (**Figure 12**) showed a significant increase in the percentage of cTnT+ cells (cardiomyocytes) in the MG-coated polyurethane acrylate nanopattern substrate (85.2 %) compared to the patterned flat substrate (77.9 %), suggesting that might be an effect of nanotopography on the differentiation efficiency of cardiomyocytes. However, the same trend is not observed when the cells were replated onto FN-coated substrates. In fact, cells that were replated onto FN-coated TCPS plates showed a significant decrease in percentage of cTnT+ cells, from 52.8 % in the control without replate group down to 36 % when cells were replated onto FN-coated TCPS substrate. As the set of data is done with a technical replicate of n = 3, further experiments to obtain biological replicates are needed to confirm if the increase in differentiation efficiency with nanotopography is consistent.

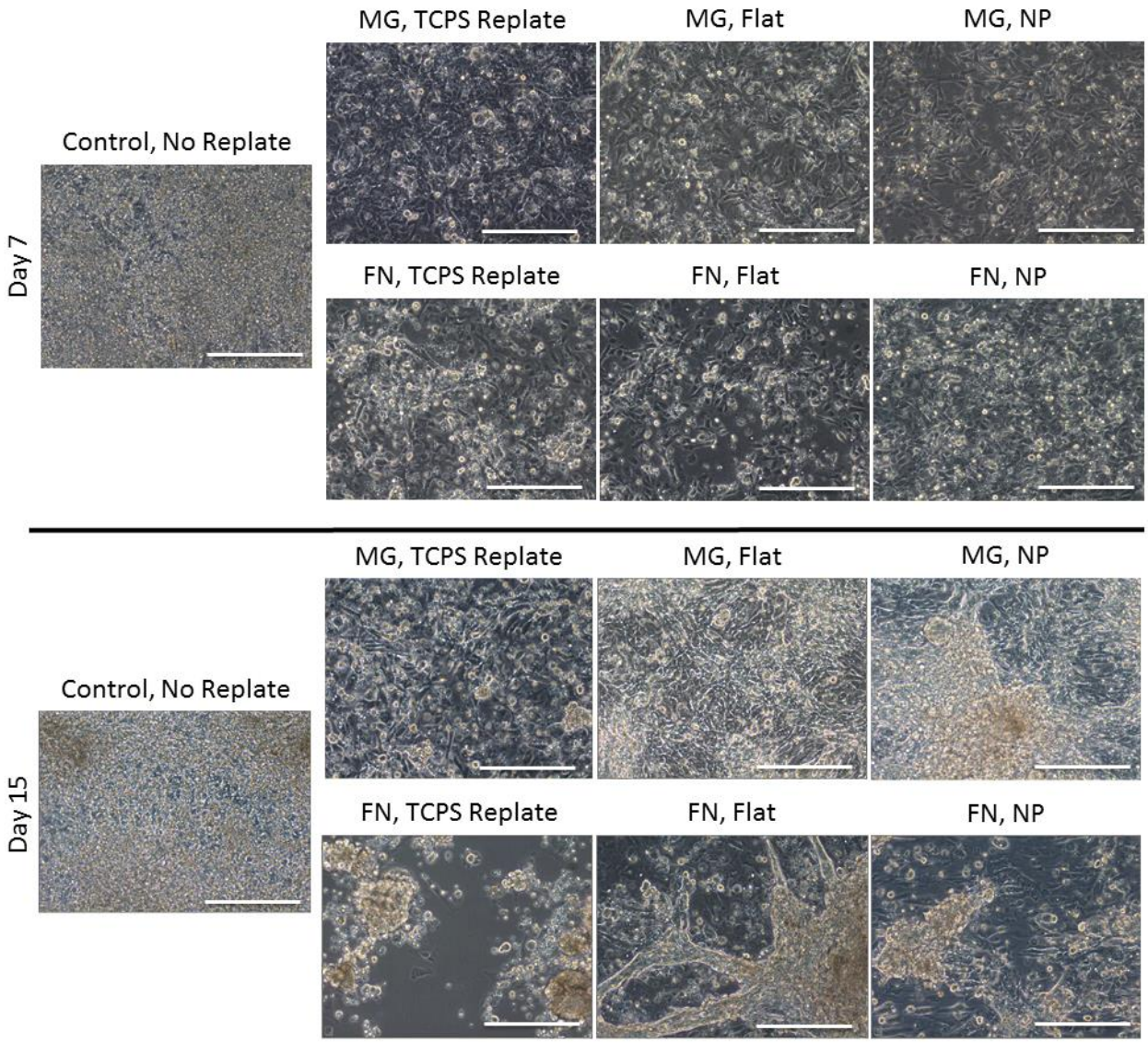

Figure 11. Introduction of nanotopographical cues at Day 6 and subsequent differentiation into cardiomyocytes. Cells were harvested from the differentiation round on Day 6 and replated onto fabricated polyurethane acrylate substrates. Cells were shown to adhere to all different substrates on Day 7, one day post replate. On day 15, cells proliferated and filled in to form a uniform, beating monolayer on MG-coated substrates. Cells did not fill in on FN-coated substrates, and cells formed clustered beating structures. Scale bars = 250 μm.

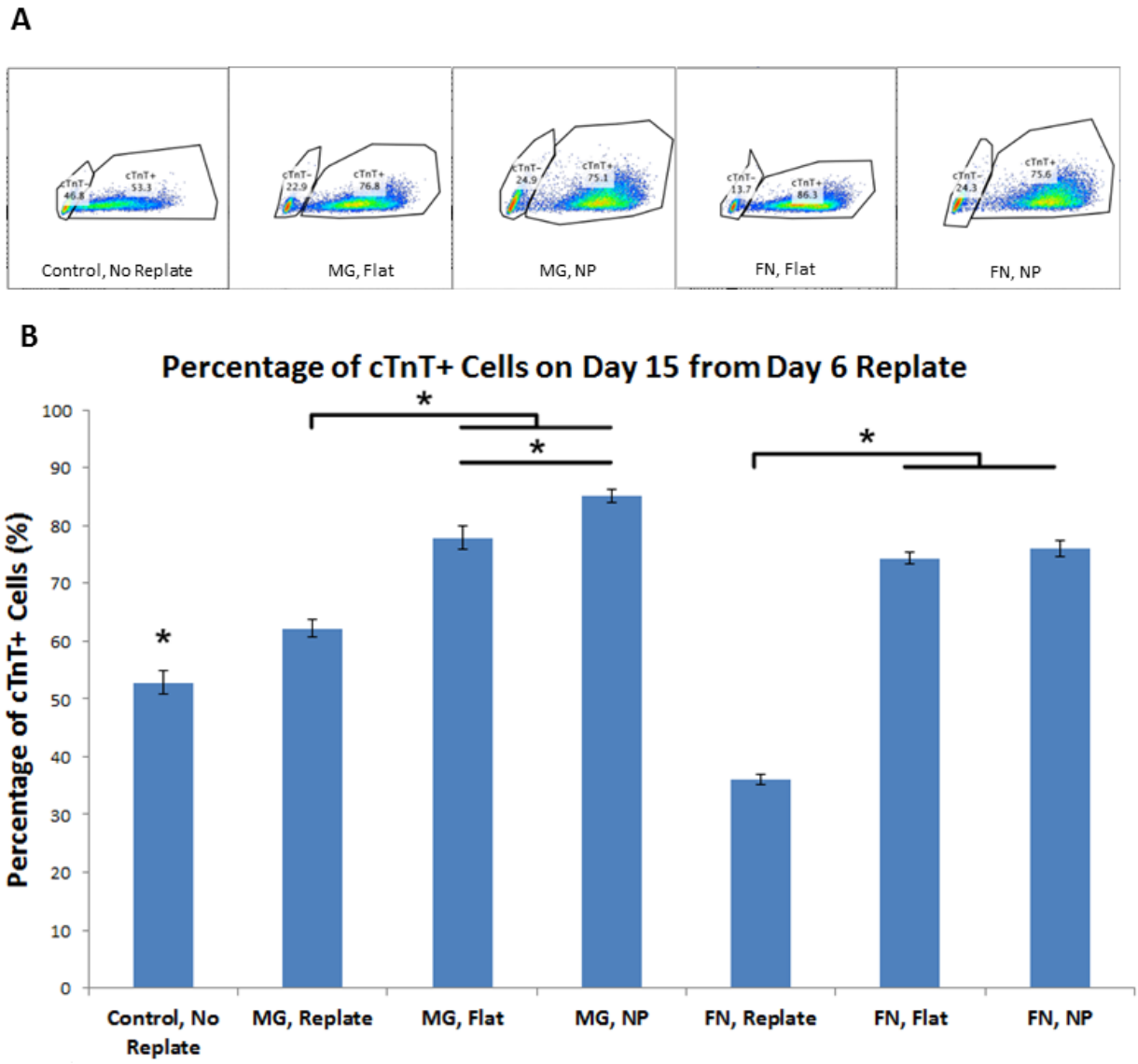

Figure 12. Flow cytometry of percentage of cTnT+ cells from each condition. Cells were differentiated until Day 6 and replated onto different substrates. Cells were harvested on Day 15 and flow cytometry was performed and gated to obtain the percentage of cTnT+ cells (**A**). (**B**) Barplot shows the mean ± SEM of the cTnT+ population measured by flow cytometry. MG-coated nanopattern significantly increased the differentiation rate of replated cells compared to the MG-coated flat substrate. This difference is not observed on the fibronectin coated substrates. * $P < 0.05$. P-values were calculated using one-way ANOVA and Tukey's HSD post hoc test.

Similarly, the same procedure was performed with a Day 8 replate. Cells were differentiated until Day 8 and replated at 500,000 cells/cm^2 onto the same substrates as from the Day 6 replate experiment. Images taken showed cells adhered to all the different substrates, and rather than forming a beating monolayer, cardiomyocytes formed beating clusters by Day 11 (**Figure 13**). Again on Day 15, dead cells were washed away with DPBS and remaining attached cells were harvested for flow cytometry for the population of alive cells (**Figure 14**). Flow data suggested that the replating procedure is detrimental to the cardiac yield of differentiating cultures, as the percentage of cTnT+ cells (cardiomyocytes) dropped from around 24.8 % in the control group (without replate) to 2.2 % in MG-TCPS and 1.2 % in FN-TCPS after replating (**Figure 14**). However, the cells that were replated onto MG- and FN- coated fabricated substrate on polyurethane acrylate polymer experienced higher differentiation efficiency. For example, the cells replated onto MG-coated patterned flat and nanopatterns achieved efficiencies of around 14.7 % and 13.5 %, respectively, while those on FN-coated patterned flat and nanopatterns had efficiencies of 7.4 % and 8.4 %, respectively. However, the differences in these groups between flat and nanopattern were not of statistical significance. Nonetheless, it suggested that differentiation of CPCs into cardiomyocytes on nanotopography was possible and enhanced as compared to the replated controls. The results also suggested that cells performed better on Matrigel-coated substrate than fibronectin-coated substrates. The lower efficiencies could also be due to the differentiation protocol being optimized to MG-TCPS conditions.

Overall, the results showed hints of improved cardiac differentiation efficiency with nanotopographical with an increase in cTnT+ cells in the MG-coated group from Day 6 replate. However, there were no difference between flat and nanotopography from Day 8 replate group, and the replating procedure with enzymatic digestion of cells appeared to have negative effects

on cardiac differentiation efficiency. During the differentiation process, the cell population is highly dynamic in cell type composition and stages of lineage differentiation. The Day 6 and Day 8 replate had very different results despite the same experimental parameters. For example, replating the cells at Day 8 of differentiation resulted in sharp decrease in final percentage of cardiomyocytes on Day 15, whereas replating on Day 6 showed increased percentage of cardiomyocytes compared to control on MG-coated substrates. Thus, this suggested that the cell population responded to the replating procedure with enzymatic digestion very differently at different time points, which introduced an extra variable in this study, undermining the ability to directly compare the results from different time points.

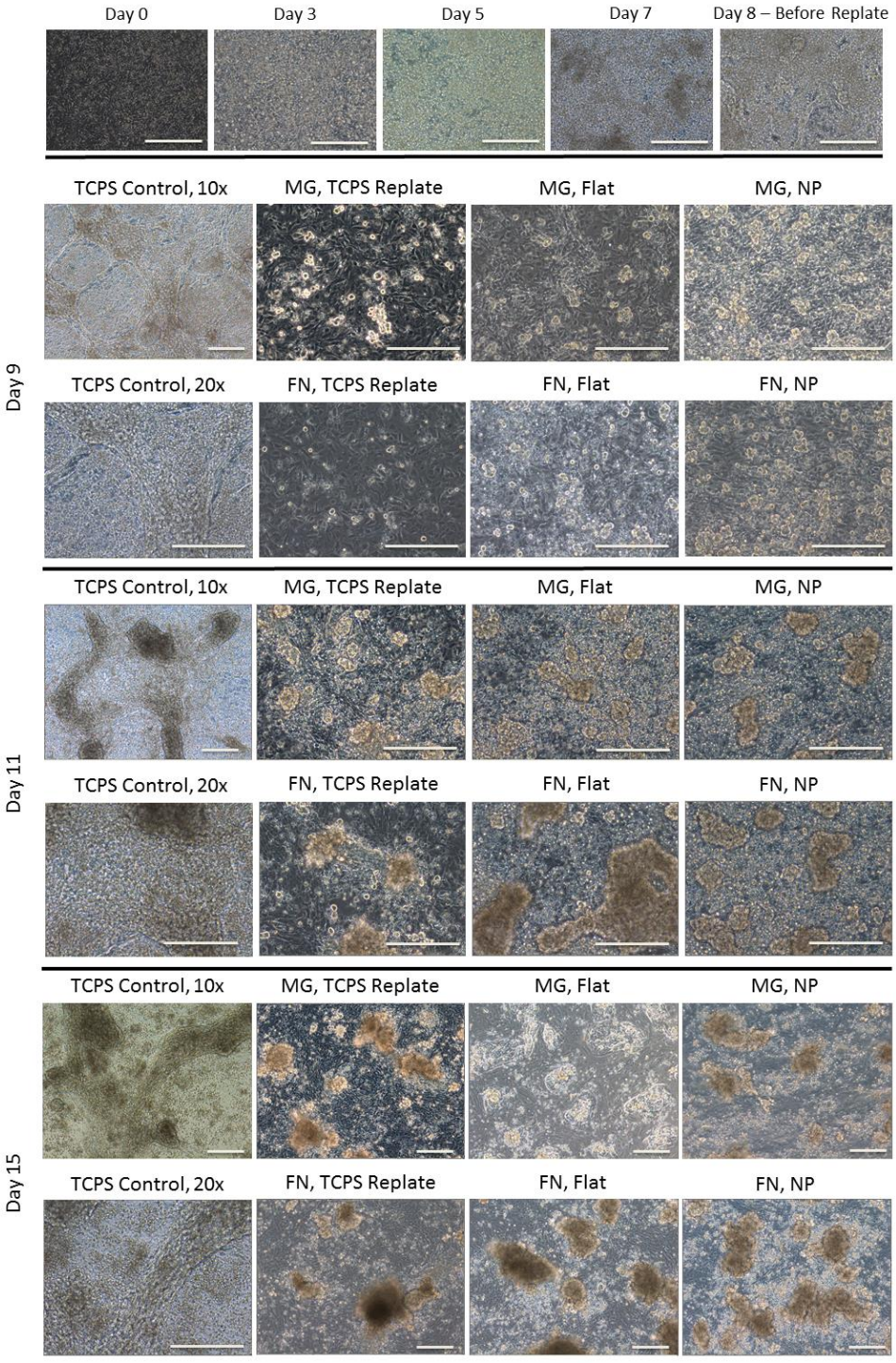

Figure 13. Introduction of nanotopographical cues at Day 8 and subsequent differentiation into cardiomyocytes. The differentiation process of cardiomyocytes was closely monitored. Cells were shown to adhere to all different substrates, and all substrate conditions had cells that exhibited beating by Day 11. However, cardiomyocytes after replate formed beating clusters instead of a beating monolayer. Scale bars = 250 μm.

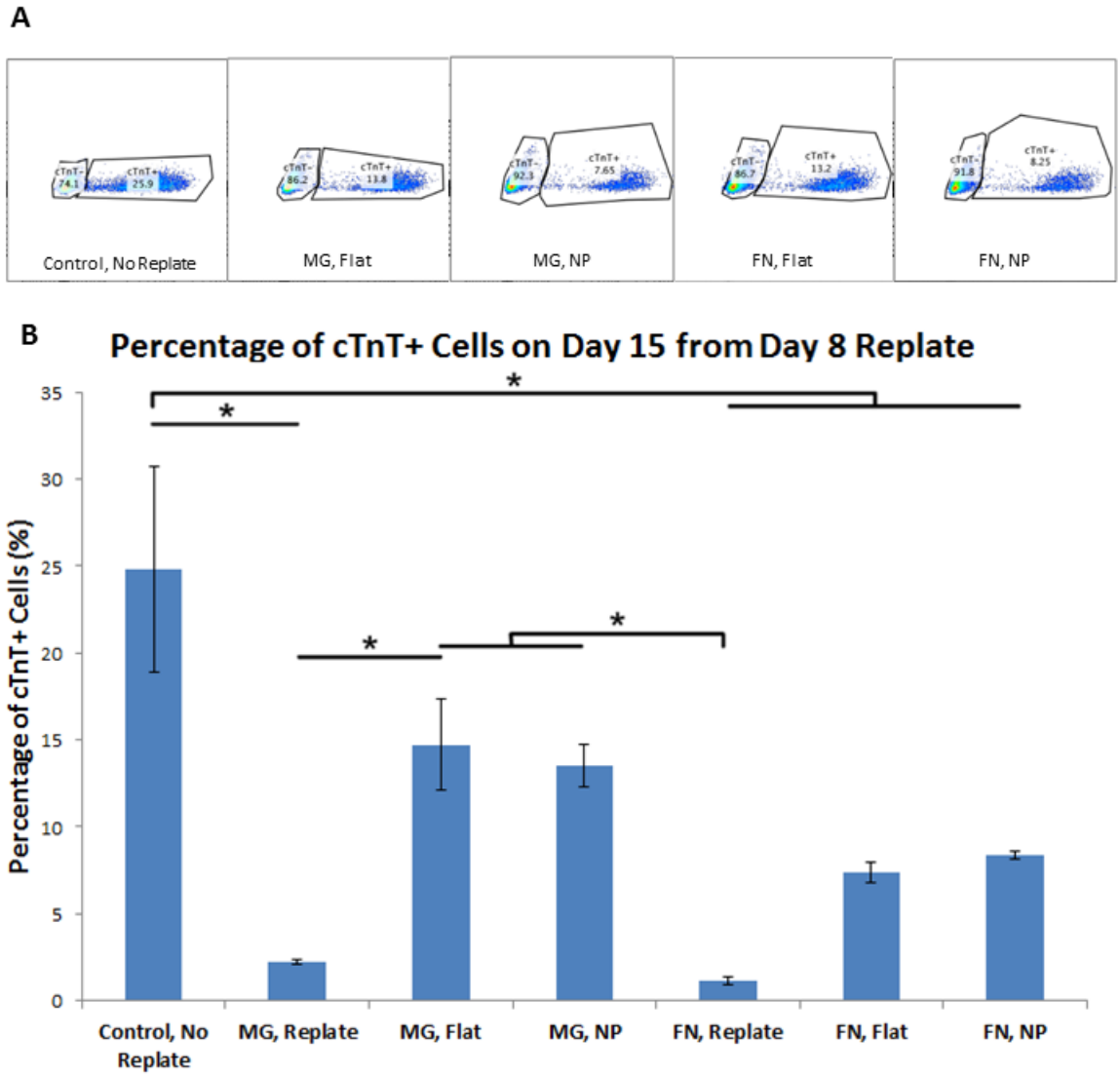

Figure 14. Percentage of cardiomyocytes on Day 15 at different substrates for CPC differentiation into cardiomyocytes. Cells were differentiated until Day 8 and replated onto different substrates. Cells were harvested on Day 15 and flow cytometry was performed and gated to obtain the percentage of cTnT+ cells (**A**). (**B**) Barplot shows the mean ± SEM of the cTnT+ population measured by flow cytometry. Cells differentiated on MG-coated TCPS without replate achieved around 25% cardiomyocyte efficiency, while cells that were replated onto MG-coated and FN-coated TCPS showed a significant decrease in percentage of cTnT+ cells on Day 15, suggesting that the replating procedure is detrimental to the differentiation process. Cells that were replated onto MG-coated and FN-coated flat and nanopatterns were shown to achieve higher differentiation efficiency when compared to their corresponding replate controls on TCPS, but differences between flat and nanopattern were not of statistical significance. Cells grown on MG-coated fabricated substrates also appeared to differentiate better than FN-coated fabricated substrates, although this difference is also not of statistical significance. Plotted are means ± standard errors. * $P < 0.05$. P-values were calculated using one-way ANOVA and Tukey's HSD post hoc test.

Strategy 2: Introduction of nanotopography with memory shape polymer through photothermal effects.

As the data from strategy 1 suggested that the cell population responds to the replating procedure very differently at different timepoints, there is a need to introduce the nanotopographical cues without the enzymatic digestion of cells. Hence, the solution is to fabricate a memory shape polymer to introduce the nanotopography via photothermal effect. For this project, poly(ε-caprolactone) (PCL) was chosen for its biocompatibility as well as dual-shape capability [82, 83]. PCL falls in the category of smart materials that can change from temporary to permanent shape with the application of an external stimulus [84, 85]. The PCL polymer would start off with a permanent shape with regions of high crystallinity and amorphous region; upon heating of the polymer to its melting temperature, the whole polymer will turn amorphous, at which stage it can be deformed into a temporary shape (**Figure 15**). With the deformation, the polymer can be cooled down to crystalize the structure and to retain the temporary shape, until the polymer is heated to its melting temperature again to return to the permanent shape. The PCL polymers were crosslinked from two different macromolecules: a tetra-branched PCL (4b10PCL) and a two-branced PCL (2b20PCL). By crosslinking different ratios of these two macromolecules, different polymer temperature could be achieved [86-89]. For the purpose of this experiment, a melting temperature slightly above physiological temperature of 37^{o}C was chosen, which corresponded to an 80:20 ratio of 2b20PCL:4b10PCL.

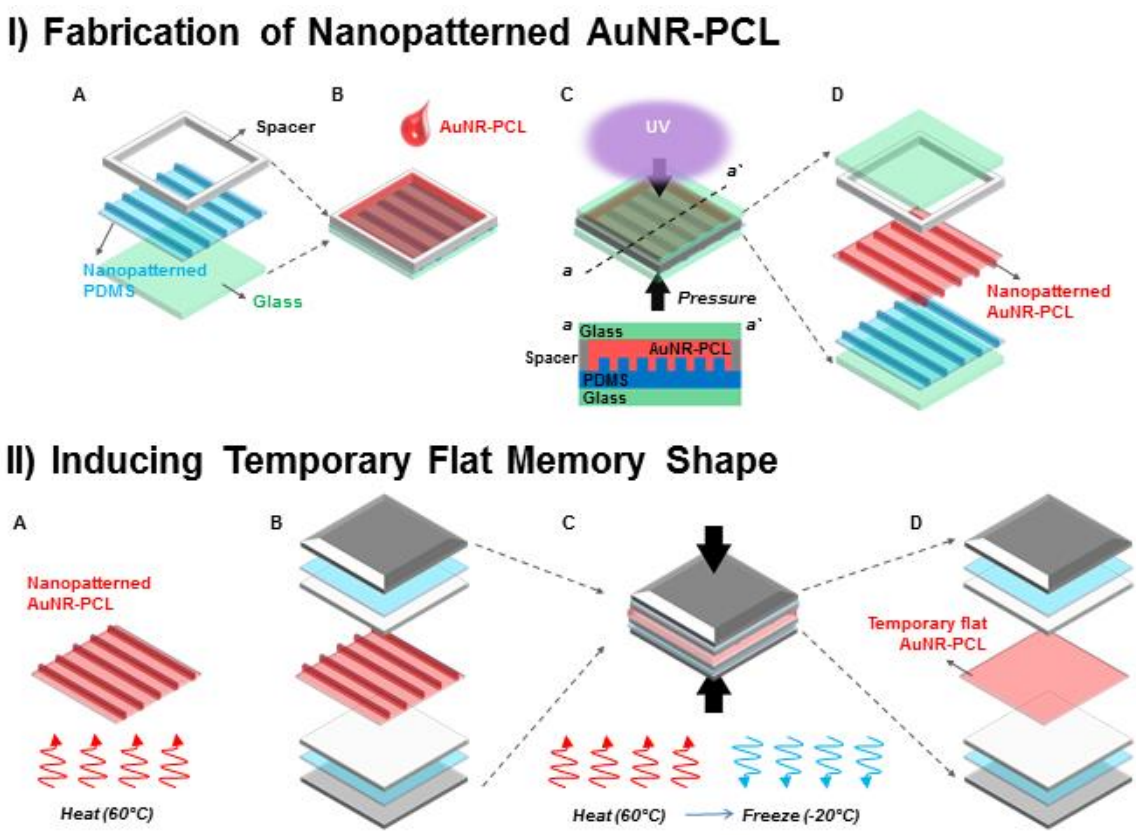

Figure 15. Fabrication of AuNR-PCL smart materials. The fabrication of a permanent topography starts the addition of AuNR-PCL polymer onto a PDMS mold with a spacer (**I. A&B**). The polymer is then sandwiched between two glass slides and UV cured (**I. C**) and peeled off to obtain the nanopatterned AuNR-PCL (**I. D**). To induce a temporary shape, the nanopatterned AuNR-PCL polymer was heated (**II. A**) and sandwiched between two flat Teflon sheets, PDMS cushion blocks, and metal plates (**II. B**). Upon the application of pressure to deform and flatten the polymer (**II. C**), the polymer crystallizes and result in a temporary flat topography (**II. D**).

Gold nanorods (AuNR) were also incorporated into the polymer. AuNR was chosen for its biocompatibility and photothermal effects. AuNR has peak absorption at near infrared spectrum around 800nm, and this property allows localized heating of the AuNR-PCL polymer with a focused NIR beam [76]. It has also been shown that the temperature at which the polymer would plateau upon light treatment is dependent on the light source intensity, which would

prevent the polymer from overheating, causing side effects such as heat shocking the cells grown on it.

In this chapter, different amounts of AuNR were incorporated into the fabrication of PCL, at 0 %, 0.5 %, 1 %, and 3 %. It was found that at 3% AuNR, the polymer became too pigment-dense; upon UV treatment, UV light could not penetrate the polymer well, and the polymer did not crosslink well. However, the AuNR-PCL at 0%, 0.5%, and 1% crosslinked with no problem. The AuNR-PCL polymers were fabricated with a PDMS mold to incur a permanent shape with nanotopography. A temporary shape was then induced by applying pressure to the polymer sandwiched between flat Teflon sheets, PDMS blocks, and two metal plates to deform and flatten the nanotopographical features on the polymer. Upon the cooling and crystallization of the deformed/flattened polymer, a temporary shape is retained. To induce a shape change back to nanotopography, a strong studio lamp was used in replacement of the ideal NIR light source. It took around 17 seconds to induce a topography change from flat to pattern in PCL with no AuNR. The topography change could be indicated by the appearance of a rainbow colored surface, as the 800nm nanogrooves and nanoridges diffracts light (**Figure 16**). On the other hand, the AuNR-PCL with 0.5 %, 1 %, and 3 % AuNR took only about 7 seconds of light irradiation time to achieve a change in topography. The decreased light irradiation time upon the addition of AuNR allow the polymer's exposure to the photothermal effect to be minimized, which is beneficial to cell studies to minimize the exposure to potential harm to the cells from heating.

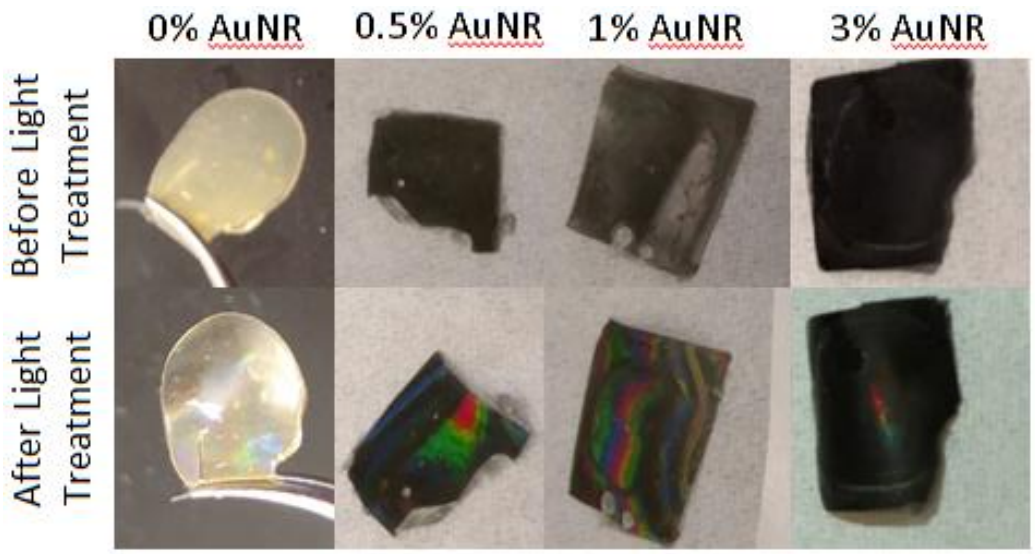

Figure 16. Before and after images of AuNR-PCL upon light treatment. Upon light treatment from a strong studio lamp (17 s for PCL without AuNR, and 7 s for PCL with AuNR), the polymers underwent a topographical change from flat to patterned. This was indicated by the appearance of a rainbow color caused by the diffraction of light from the 800nm nanogrooves and nanoridges of the pattern.

Next, cells were tested on whether they remain attached to the polymer upon a topographical change. To achieve this, PCL substrates were fabricated and a temporary flat shape was induced by deforming the polymer with a clamp and a crystallization process. The PCL substrates were then plasma treated to make the surface hydrophilic, UV sterilized, and coated with Matrigel. UC3-4 colonies were then plated onto the polymers and grown overnight to allow attachment. On the next day, a photothermal effect was induced using a strong studio lamp to bring the polymer past its melting temperature (about 7 seconds). The polymers with cells were immediately washed in PBS twice to get rid of any detached cells and fixed in 4% paraformaldehyde for immunostaining of nucleus, F-actin, and vinculin (**Figure 17**). Confocal images showed that upon the topographical change, cells still remained attached. However, these images were not able to show that the cells' cytoskeleton became aligned to the substrate, as they

were probably not given enough time to rearrange their cytoskeleton being immediately washed and fixed. Finally, to confirm that nanotopography was truly introduced, scanning electron microscopy (SEM) was used to image the topography of the polymers that cells were grown on (**Figure 18**). Compared to the AuNR-PCL receiving no light treatment, the AuNR-PCL with light treatment showed the emergence of the expected nanotopography, featured by nanogrooves and nanoridges.

To summarize the second strategy, the fabrication process of a photothermal-responsive smart material was developed to induce a topographical change from flat to nanopattern with a light stimulus. It had been shown that incorporating AuNR into PCL could decrease the amount of light irradiation time needed to induce a topographical change. Cells were also seeded onto the PCL substrates and shown to remain attached upon light irradiation and topographical change of the substrate.

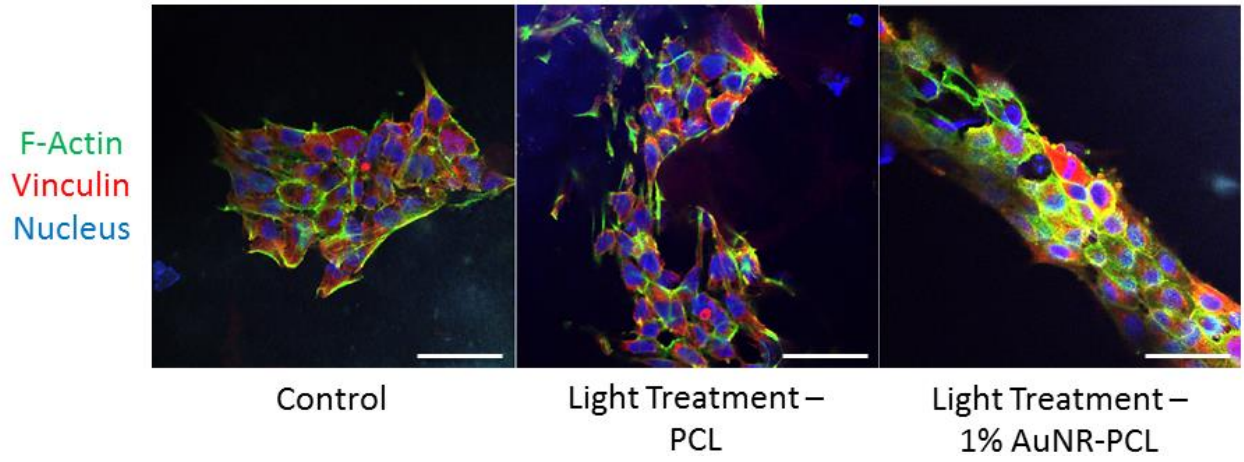

Figure 17. Confocal images of cells seeded on PCL substrates. PCL substrates were made with and without AuNR incorporation. Cells were seeded on the PCL polymers at their temporary, flattened shape. Upon light treatment (17 s for PCL and 7 s for 1 % AuNR-PCL), cells were shown to still remain attached. Scale bars = 50 μm.

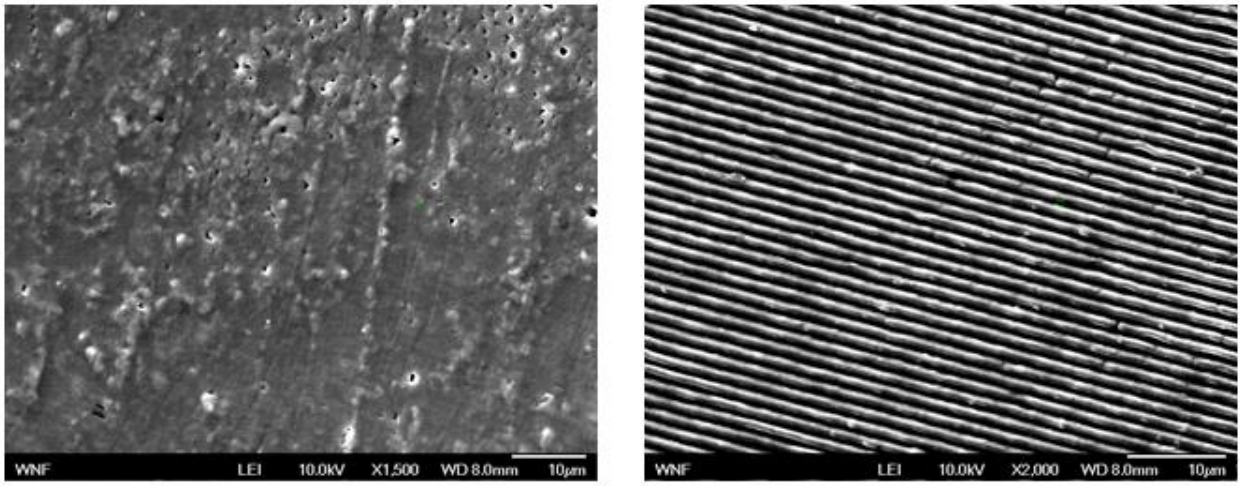

Figure 18. SEM images of PCL polymers. Compared to the control group with no light treatment, the 1 % AuNR-PCL receiving light treatment showed the emergence of the fabricated permanent shape with nanogrooves and nanoridges, confirming the introduction of nanotopographical cues to the cells that were seeded on them.

3.4 Discussion

Besides regulating cell morphology and function, cell-matrix adhesion complexes have also been shown to determine cell fate through mechanotransduction, as mentioned in the background section. Thus, this chapter was focused on the effect of nanotopography on the differentiation of cardiomyocytes. It was hypothesized that the introduction of nanotopographical cues at the cardiac progenitor stage would enhance the differentiation efficiency of cardiomyocytes. Again, the nanotopographical cues were introduced at this stage because cells were converting from cardiac mesoderm to cardiac progenitor cells, which is a logical stage to introduce cues biomimetic to that in the native myocardium. Introducing these cues too early when they are still stem cells might set off different signaling cascades that can drive them down the wrong lineage as stem cells are not normally exposed to the cues from the native

myocardium. With the first strategy, the cell population that was replated on Day 6 onto patterend polyurethane acrylate substrates showed an increase in the percentage of cTnT+ cells (cardiomyocytes) at Day 15 of differentiation on MG-coated substrates, suggesting the introduction of nanotopography might have an effect in either 1) selecting and promoting the proliferation of cardiac progenitor cells that could differentiate into cardiomyocytes, and/or 2) improving the differentiation efficiency of cardiomyocytes from cardiac progenitor cells. Next, replating the cell population on Day 8 of differentiation showed drastic difference in cardiac efficiency by Day 15, with results suggesting that the replating procedure is detrimental to the final yield of cardiomyocytes. Together, this showed that the dynamic cell population undergoing differentiation responds very differently to the replating procedure with enzymatic digestion of the cells, which disrupt the cell-cell contact shown to be important during the differentiation of cardiomyocytes and for cell-cell signaling that could activate differentiation-associated genes and alter genotype and phenotype [80]. From the Day 8 replate group, there were no difference in the final percentage of cardiomyocytes between patterned flat and nanopatterned substrates. These were done in technical replicates of n = 3, and more experiments with biological replicates are needed to confirm consistency and reproducibility of the data before any strong conclusions can be drawn. It should also be noted that as the cell population responded differently to the replating procedure at different time points, it added an extra variable, preventing a straight comparison between the results from the two different days of replate. Thus, this motivates a second strategy to be developed to introduce the nanotopographical cues in a more controlled manner.

In the second strategy, a photothermal-responsive material was developed using AuNR incorporated into PCL polymer. A melting temperature of the polymer slightly above the

physiological temperature was achieved, and the addition of AuNR effectively decreased the irradiation time necessary to incur a topographical change. SEM images have confirmed the topographical change from flat to nanopattern with the emergence of nanoridges and nanogroove, and immunostained images of the cells on the polymers had confirmed that cells remained attached the substrates upon the light treatment of the polymer. With the successful development of this AuNR-PCL platform, the introduction of nanotopography to the cells can be easily manipulated with a light source, and this negated the need to enzymatically digest the cells for replate. Thus in future experiments utilizing this platform, the results between the flat and nanopattern group at different time points can be attributed to the introduction of nanotopography, and it allows a direct comparison between the different time points.

Chapter 4: Conclusions and Future Works

4.1 Summary of Work

Based on the premise that cell-matrix interaction is bi-directional and that cells can sense and respond to the cues in the extracellular matrix, the effects of nanotopography on the structural maturation and differentiation of cardiomyocytes were investigated. This served to address the current limitation of immature phenotypes displayed by hiPSC-derived cardiomyocytes and the need to drive the maturation of cardiomyocytes for their applicability in regenerative medicine, disease modeling, and drug screening. It had been shown that nanotopography promoted the structural organization and maturation of cardiomyocytes, with an increase in F-actin alignment, cell anisotropic ratio, sarcomeric length, banding formation, and Z-band width. However, the effects of T3 on these parameters were not clear, and data from Week 3 suggested the prolonged exposure of an elevated level of T3 can have detrimental effects in decreasing cell area and elongation. Thus, testing the optimal treatment time and concentration of T3 is the logical next step. Introduction of nanotopography during the differentiation procedure with a Day 6 replate onto polyurethane acrylate polymers showed improvement of nanotopography on the differentiation efficiency of cardiomyocytes. Data from the Day 8 replate suggested replating at this developmental stage can be detrimental to the cardiomyocyte differentiation efficiency. Hence, the differentiating cell population is highly dynamic and responds to the replating procedure vastly different at different time points, which can introduce an extra variable to the experimental design. Therefore, a photothermal-responsive polymer was developed that could change topography from flat to nanopattern with light irradiation. Cells have been shown to remain attached to the polymers after light irradiation and a topography change from flat to nanopattern. Thus, the platform allows for easy manipulation of a

topographical change with light irradiation and has vast potentials in future cell studies involving the introduction of nanotopography in the extracellular matrix.

4.2 Future Studies

In retrospect, there were aspects of the research design that could have been improved on. In the cardiomyocyte maturation study, the level of T3 could have been optimized to find the ideal concentration and exposure time. Currently, the data suggested that the dosage level of T3 used induced cytotoxic effects, undermining the ability of the experiment to test the effect of T3 on cardiomyocyte maturation combined with nanotopographical cues. Optimizing the concentration of T3 as well as testing more exposure time points (such as a one-week treatment) would give a better insight on whether T3 have synergistic effects with nanotopography on the maturation of cardiomyocytes as well as its effects over time. Conversely, this platform can give interesting insights to answer biological questions involving the effects of an elevated level of T3, a condition known as hyperthyroidism. Hyperthyroidism has been associated with tachycardia, atrial fibrillation, hypertension, coronary artery disease, and heart failure [90]. However, long-term effects of hyperthyroidism on cardiac function and metabolism is not completely known [73]. Thus, with the current platform that has been shown to be responsive to prolonged hyperthyroidism, cardiac tissues grown on nanotopography can be subjected to an elevated level of T3 over time to be characterized structurally and functionally.

In the cardiac differentiation study, a limitation was that the cells were not profiled over the differentiation process. The differentiation stage of the cell population at the point of nanotopography introduction could only be deduced from literature that had characterized the same differentiation protocol. Similarly, the composition of the cell population was also unknown. Profiling the cell population with stem cell and cardiac progenitor cell markers using

flow cytometry or a reporter cell line would give valuable information. For example, the cell types present at the time of nanotopography introduction could be identified to draw conclusion on the optimal stage of differentiation for introducing nanotopographical cues. A cell viability test would help to answer whether an increase in cTnT+ cells could be truly attributed to the introduction of nanotopographical cues or if it was from apoptosis of non-cardiac fated cells during the replate procedure.

To move the PCL platform forward, there are different directions that could be taken. First, differentiation conditions on the AuNR-PCL polymers need to be optimized. This is especially important because the polymers are opaque and does not allow light to pass through under the microscope, which poses a challenge because ensuring that a confluent monolayer is achieved is critical for the differentiation induction time point. Current protocols are optimized for the TCPS culture condition, and optimizing the protocol for the AuNR-PCL substrates would help to achieve good differentiation rounds.

Next, it would be interesting to use this platform to find the optimal time of nanotopography introduction that would result in the best cardiac differentiation efficiency. In conjunction with this project, reporter cells lines could also be utilized marking for the Nkx2.5 and Isl1 markers to confirm the stage of the cells at the time of nanotopography introduction. Alternatively, a Wnt reporter cell line can also be used to probe the activities of Wnt activation and deactivation, and this can be used to study the effects of introducing the effects of nanotopography on the Wnt activities, which is a major regulator of the differentiation process of stem cells into cardiac mesoderm, cardiac progenitor cells, and cardiomyocytes. Cells can also be differentiated on this platform and carried out to the same maturation endpoints as in Chapter 2

to test whether introducing the nanotopographical cues earlier on can mature cardiomyocytes faster and to a greater extent.

Finally, future experiments can also focus on characterizing the differentiation process. For instance, stable hiPSC lines that are fluorescently tagged (such as with α-actinin) could be utilized and imaged regularly with live-cell microscopy to characterize and investigate the cytoskeletal development and changes upon the introduction of the nanotopography during differentiation. Another approach would be to plate an established cardiac progenitor cell line directly onto the patterned substrates to test the effects of nanotopography on cardiac differentiation yield and efficiency. All in all, there are many potential experiments that can be performed to address the limitations of the studies as well as investigate further biological questions.

References

1. Ebert AD, Liang P, Wu JC: Induced pluripotent stem cells as a disease modeling and drug screening platform. *J Cardiovasc Pharmacol* 2012, 60:408-416.
2. Takahashi K, Yamanaka S: Induction of pluripotent stem cells from mouse embryonic and adult fibroblast cultures by defined factors. *Cell* 2006, 126:663-676.
3. Zhou T, Benda C, Dunzinger S, Huang Y, Ho JC, Yang J, Wang Y, Zhang Y, Zhuang Q, Li Y, et al: Generation of human induced pluripotent stem cells from urine samples. *Nat Protoc* 2012, 7:2080-2089.
4. Moretti A, Laugwitz KL, Dorn T, Sinnecker D, Mummery C: Pluripotent stem cell models of human heart disease. *Cold Spring Harb Perspect Med* 2013, 3.
5. Liang P, Lan F, Lee AS, Gong T, Sanchez-Freire V, Wang Y, Diecke S, Sallam K, Knowles JW, Wang PJ, et al: Drug screening using a library of human induced pluripotent stem cell-derived cardiomyocytes reveals disease-specific patterns of cardiotoxicity. *Circulation* 2013, 127:1677-1691.
6. Classen DC, Pestotnik SL, Evans RS, Lloyd JF, Burke JP: Adverse drug events in hospitalized patients. Excess length of stay, extra costs, and attributable mortality. *JAMA* 1997, 277:301-306.
7. Kehat I, Kenyagin-Karsenti D, Snir M, Segev H, Amit M, Gepstein A, Livne E, Binah O, Itskovitz-Eldor J, Gepstein L: Human embryonic stem cells can differentiate into myocytes with structural and functional properties of cardiomyocytes. *J Clin Invest* 2001, 108:407-414.
8. Guilak F, Cohen DM, Estes BT, Gimble JM, Liedtke W, Chen CS: Control of stem cell fate by physical interactions with the extracellular matrix. *Cell Stem Cell* 2009, 5:17-26.
9. Kshitiz, Park J, Kim P, Helen W, Engler AJ, Levchenko A, Kim DH: Control of stem cell fate and function by engineering physical microenvironments. *Integr Biol (Camb)* 2012, 4:1008-1018.
10. McBeath R, Pirone DM, Nelson CM, Bhadriraju K, Chen CS: Cell shape, cytoskeletal tension, and RhoA regulate stem cell lineage commitment. *Dev Cell* 2004, 6:483-495.
11. Reilly GC, Engler AJ: Intrinsic extracellular matrix properties regulate stem cell differentiation. *J Biomech* 2010, 43:55-62.
12. Darribère T, Schwarzbauer JE: Fibronectin matrix composition and organization can regulate cell migration during amphibian development. *Mech Dev* 2000, 92:239-250.
13. Gao L, McBeath R, Chen CS: Stem cell shape regulates a chondrogenic versus myogenic fate through Rac1 and N-cadherin. *Stem Cells* 2010, 28:564-572.
14. Sordella R, Jiang W, Chen GC, Curto M, Settleman J: Modulation of Rho GTPase signaling regulates a switch between adipogenesis and myogenesis. *Cell* 2003, 113:147-158.
15. Etienne-Manneville S, Hall A: Rho GTPases in cell biology. *Nature* 2002, 420:629-635.
16. Ren XD, Kiosses WB, Schwartz MA: Regulation of the small GTP-binding protein Rho by cell adhesion and the cytoskeleton. *EMBO J* 1999, 18:578-585.
17. Seo CH, Furukawa K, Montagne K, Jeong H, Ushida T: The effect of substrate microtopography on focal adhesion maturation and actin organization via the RhoA/ROCK pathway. *Biomaterials* 2011, 32:9568-9575.
18. Ranucci CS, Moghe PV: Substrate microtopography can enhance cell adhesive and migratory responsiveness to matrix ligand density. *J Biomed Mater Res* 2001, 54:149-161.

19. Jacot JG, McCulloch AD, Omens JH: Substrate stiffness affects the functional maturation of neonatal rat ventricular myocytes. *Biophys J* 2008, 95:3479-3487.
20. Yang L, Soonpaa MH, Adler ED, Roepke TK, Kattman SJ, Kennedy M, Henckaerts E, Bonham K, Abbott GW, Linden RM, et al: Human cardiovascular progenitor cells develop from a KDR+ embryonic-stem-cell-derived population. *Nature* 2008, 453:524-528.
21. Lian X, Hsiao C, Wilson G, Zhu K, Hazeltine LB, Azarin SM, Raval KK, Zhang J, Kamp TJ, Palecek SP: Robust cardiomyocyte differentiation from human pluripotent stem cells via temporal modulation of canonical Wnt signaling. *Proc Natl Acad Sci U S A* 2012, 109:E1848-1857.
22. Metcalfe C, Bienz M: Inhibition of GSK3 by Wnt signalling--two contrasting models. *J Cell Sci* 2011, 124:3537-3544.
23. Zhang J, Klos M, Wilson GF, Herman AM, Lian X, Raval KK, Barron MR, Hou L, Soerens AG, Yu J, et al: Extracellular matrix promotes highly efficient cardiac differentiation of human pluripotent stem cells: the matrix sandwich method. *Circ Res* 2012, 111:1125-1136.
24. Paige SL, Osugi T, Afanasiev OK, Pabon L, Reinecke H, Murry CE: Endogenous Wnt/beta-catenin signaling is required for cardiac differentiation in human embryonic stem cells. *PLoS One* 2010, 5:e11134.
25. Lian X, Zhang J, Azarin SM, Zhu K, Hazeltine LB, Bao X, Hsiao C, Kamp TJ, Palecek SP: Directed cardiomyocyte differentiation from human pluripotent stem cells by modulating Wnt/β-catenin signaling under fully defined conditions. *Nat Protoc* 2013, 8:162-175.
26. Li D, Zhou J, Wang L, Shin ME, Su P, Lei X, Kuang H, Guo W, Yang H, Cheng L, et al: Integrated biochemical and mechanical signals regulate multifaceted human embryonic stem cell functions. *J Cell Biol* 2010, 191:631-644.
27. Engler AJ, Sen S, Sweeney HL, Discher DE: Matrix elasticity directs stem cell lineage specification. *Cell* 2006, 126:677-689.
28. Laflamme MA, Murry CE: Heart regeneration. *Nature* 2011, 473:326-335.
29. Drouin E, Charpentier F, Gauthier C, Laurent K, Le Marec H: Electrophysiologic characteristics of cells spanning the left ventricular wall of human heart: evidence for presence of M cells. *J Am Coll Cardiol* 1995, 26:185-192.
30. Gerdes AM, Kellerman SE, Moore JA, Muffly KE, Clark LC, Reaves PY, Malec KB, McKeown PP, Schocken DD: Structural remodeling of cardiac myocytes in patients with ischemic cardiomyopathy. *Circulation* 1992, 86:426-430.
31. Bird SD, Doevendans PA, van Rooijen MA, Brutel de la Riviere A, Hassink RJ, Passier R, Mummery CL: The human adult cardiomyocyte phenotype. *Cardiovasc Res* 2003, 58:423-434.
32. Ziman AP, Gómez-Viquez NL, Bloch RJ, Lederer WJ: Excitation-contraction coupling changes during postnatal cardiac development. *J Mol Cell Cardiol* 2010, 48:379-386.
33. Brodsky VYa, Chernyaev AL, Vasilyeva IA: Variability of the cardiomyocyte ploidy in normal human hearts. *Virchows Arch B Cell Pathol Incl Mol Pathol* 1991, 61:289-294.
34. Itzhaki I, Rapoport S, Huber I, Mizrahi I, Zwi-Dantsis L, Arbel G, Schiller J, Gepstein L: Calcium handling in human induced pluripotent stem cell derived cardiomyocytes. *PLoS One* 2011, 6:e18037.

35. Germanguz I, Sedan O, Zeevi-Levin N, Shtrichman R, Barak E, Ziskind A, Eliyahu S, Meiry G, Amit M, Itskovitz-Eldor J, Binah O: Molecular characterization and functional properties of cardiomyocytes derived from human inducible pluripotent stem cells. *J Cell Mol Med* 2011, 15:38-51.
36. Lundy SD, Zhu WZ, Regnier M, Laflamme MA: Structural and functional maturation of cardiomyocytes derived from human pluripotent stem cells. *Stem Cells Dev* 2013, 22:1991-2002.
37. Zhang D, Shadrin IY, Lam J, Xian HQ, Snodgrass HR, Bursac N: Tissue-engineered cardiac patch for advanced functional maturation of human ESC-derived cardiomyocytes. *Biomaterials* 2013, 34:5813-5820.
38. Mihic A, Li J, Miyagi Y, Gagliardi M, Li SH, Zu J, Weisel RD, Keller G, Li RK: The effect of cyclic stretch on maturation and 3D tissue formation of human embryonic stem cell-derived cardiomyocytes. *Biomaterials* 2014, 35:2798-2808.
39. Negro A, Boehm M: Cardiomyocyte maturation: It takes a village to raise a kid. *J Mol Cell Cardiol* 2014, 74:193-195.
40. Sartiani L, Bettiol E, Stillitano F, Mugelli A, Cerbai E, Jaconi ME: Developmental changes in cardiomyocytes differentiated from human embryonic stem cells: a molecular and electrophysiological approach. *Stem Cells* 2007, 25:1136-1144.
41. Kamakura T, Makiyama T, Sasaki K, Yoshida Y, Wuriyanghai Y, Chen J, Hattori T, Ohno S, Kita T, Horie M, et al: Ultrastructural maturation of human-induced pluripotent stem cell-derived cardiomyocytes in a long-term culture. *Circ J* 2013, 77:1307-1314.
42. Caspi O, Lesman A, Basevitch Y, Gepstein A, Arbel G, Habib IH, Gepstein L, Levenberg S: Tissue engineering of vascularized cardiac muscle from human embryonic stem cells. *Circ Res* 2007, 100:263-272.
43. Engelmayr GC, Cheng M, Bettinger CJ, Borenstein JT, Langer R, Freed LE: Accordion-like honeycombs for tissue engineering of cardiac anisotropy. *Nat Mater* 2008, 7:1003-1010.
44. Silvestri A, Boffito M, Sartori S, Ciardelli G: Biomimetic Materials and Scaffolds for Myocardial Tissue Regeneration. *Macromol Biosci* 2013.
45. Stevens KR, Kreutziger KL, Dupras SK, Korte FS, Regnier M, Muskheli V, Nourse MB, Bendixen K, Reinecke H, Murry CE: Physiological function and transplantation of scaffold-free and vascularized human cardiac muscle tissue. *Proc Natl Acad Sci U S A* 2009, 106:16568-16573.
46. Stevens KR, Pabon L, Muskheli V, Murry CE: Scaffold-free human cardiac tissue patch created from embryonic stem cells. *Tissue Eng Part A* 2009, 15:1211-1222.
47. Kensah G, Roa Lara A, Dahlmann J, Zweigerdt R, Schwanke K, Hegermann J, Skvorc D, Gawol A, Azizian A, Wagner S, et al: Murine and human pluripotent stem cell-derived cardiac bodies form contractile myocardial tissue in vitro. *Eur Heart J* 2013, 34:1134-1146.
48. Tulloch NL, Muskheli V, Razumova MV, Korte FS, Regnier M, Hauch KD, Pabon L, Reinecke H, Murry CE: Growth of engineered human myocardium with mechanical loading and vascular coculture. *Circ Res* 2011, 109:47-59.
49. Schaaf S, Shibamiya A, Mewe M, Eder A, Stöhr A, Hirt MN, Rau T, Zimmermann WH, Conradi L, Eschenhagen T, Hansen A: Human engineered heart tissue as a versatile tool in basic research and preclinical toxicology. *PLoS One* 2011, 6:e26397.

50. Habib M, Shapira-Schweitzer K, Caspi O, Gepstein A, Arbel G, Aronson D, Seliktar D, Gepstein L: A combined cell therapy and in-situ tissue-engineering approach for myocardial repair. *Biomaterials* 2011, 32:7514-7523.
51. Zimmermann WH, Schneiderbanger K, Schubert P, Didié M, Münzel F, Heubach JF, Kostin S, Neuhuber WL, Eschenhagen T: Tissue engineering of a differentiated cardiac muscle construct. *Circ Res* 2002, 90:223-230.
52. Heidi Au HT, Cui B, Chu ZE, Veres T, Radisic M: Cell culture chips for simultaneous application of topographical and electrical cues enhance phenotype of cardiomyocytes. *Lab Chip* 2009, 9:564-575.
53. Sathaye A, Bursac N, Sheehy S, Tung L: Electrical pacing counteracts intrinsic shortening of action potential duration of neonatal rat ventricular cells in culture. *J Mol Cell Cardiol* 2006, 41:633-641.
54. Nunes SS, Miklas JW, Liu J, Aschar-Sobbi R, Xiao Y, Zhang B, Jiang J, Massé S, Gagliardi M, Hsieh A, et al: Biowire: a platform for maturation of human pluripotent stem cell-derived cardiomyocytes. *Nat Methods* 2013, 10:781-787.
55. Deng XF, Rokosh DG, Simpson PC: Autonomous and growth factor-induced hypertrophy in cultured neonatal mouse cardiac myocytes. Comparison with rat. *Circ Res* 2000, 87:781-788.
56. Földes G, Mioulane M, Wright JS, Liu AQ, Novak P, Merkely B, Gorelik J, Schneider MD, Ali NN, Harding SE: Modulation of human embryonic stem cell-derived cardiomyocyte growth: a testbed for studying human cardiac hypertrophy? *J Mol Cell Cardiol* 2011, 50:367-376.
57. Lee YK, Ng KM, Chan YC, Lai WH, Au KW, Ho CY, Wong LY, Lau CP, Tse HF, Siu CW: Triiodothyronine promotes cardiac differentiation and maturation of embryonic stem cells via the classical genomic pathway. *Mol Endocrinol* 2010, 24:1728-1736.
58. Chattergoon NN, Giraud GD, Louey S, Stork P, Fowden AL, Thornburg KL: Thyroid hormone drives fetal cardiomyocyte maturation. *FASEB J* 2012, 26:397-408.
59. Yang X, Rodriguez M, Pabon L, Fischer KA, Reinecke H, Regnier M, Sniadecki NJ, Ruohola-Baker H, Murry CE: Tri-iodo-l-thyronine promotes the maturation of human cardiomyocytes-derived from induced pluripotent stem cells. *J Mol Cell Cardiol* 2014, 72:296-304.
60. Montessuit C, Palma T, Viglino C, Pellieux C, Lerch R: Effects of insulin-like growth factor-I on the maturation of metabolism in neonatal rat cardiomyocytes. *Pflugers Arch* 2006, 452:380-386.
61. Kim DH, Han K, Gupta K, Kwon KW, Suh KY, Levchenko A: Mechanosensitivity of fibroblast cell shape and movement to anisotropic substratum topography gradients. *Biomaterials* 2009, 30:5433-5444.
62. Kim DH, Lipke EA, Kim P, Cheong R, Thompson S, Delannoy M, Suh KY, Tung L, Levchenko A: Nanoscale cues regulate the structure and function of macroscopic cardiac tissue constructs. *Proc Natl Acad Sci U S A* 2010, 107:565-570.
63. Li M, Iismaa SE, Naqvi N, Nicks A, Husain A, Graham RM: Thyroid hormone action in postnatal heart development. *Stem Cell Res* 2014, 13:582-591.
64. Fisher DA, Klein AH: Thyroid development and disorders of thyroid function in the newborn. *N Engl J Med* 1981, 304:702-712.

65. Xue Y, Cai X, Wang L, Liao B, Zhang H, Shan Y, Chen Q, Zhou T, Li X, Hou J, et al: Generating a non-integrating human induced pluripotent stem cell bank from urine-derived cells. *PLoS One* 2013, 8:e70573.
66. Cao N, Liang H, Huang J, Wang J, Chen Y, Chen Z, Yang HT: Highly efficient induction and long-term maintenance of multipotent cardiovascular progenitors from human pluripotent stem cells under defined conditions. *Cell Res* 2013, 23:1119-1132.
67. Kadari A, Mekala S, Wagner N, Malan D, Köth J, Doll K, Stappert L, Eckert D, Peitz M, Matthes J, et al: Robust Generation of Cardiomyocytes from Human iPS Cells Requires Precise Modulation of BMP and WNT Signaling. *Stem Cell Rev* 2014.
68. Macadangdang J, Lee HJ, Carson D, Jiao A, Fugate J, Pabon L, Regnier M, Murry C, Kim DH: Capillary force lithography for cardiac tissue engineering. *J Vis Exp* 2014.
69. Gordon AM, Huxley AF, Julian FJ: The variation in isometric tension with sarcomere length in vertebrate muscle fibres. *J Physiol* 1966, 184:170-192.
70. Ross RS, Borg TK: Integrins and the myocardium. *Circ Res* 2001, 88:1112-1119.
71. Clark EA, Brugge JS: Integrins and signal transduction pathways: the road taken. *Science* 1995, 268:233-239.
72. Schoenwaelder SM, Burridge K: Bidirectional signaling between the cytoskeleton and integrins. *Curr Opin Cell Biol* 1999, 11:274-286.
73. Degens H, Gilde AJ, Lindhout M, Willemsen PH, Van Der Vusse GJ, Van Bilsen M: Functional and metabolic adaptation of the heart to prolonged thyroid hormone treatment. *Am J Physiol Heart Circ Physiol* 2003, 284:H108-115.
74. Gessert S, Kühl M: The multiple phases and faces of wnt signaling during cardiac differentiation and development. *Circ Res* 2010, 107:186-199.
75. Moretti A, Caron L, Nakano A, Lam JT, Bernshausen A, Chen Y, Qyang Y, Bu L, Sasaki M, Martin-Puig S, et al: Multipotent embryonic isl1+ progenitor cells lead to cardiac, smooth muscle, and endothelial cell diversification. *Cell* 2006, 127:1151-1165.
76. Shou Q, Uto K, Iwanaga M, Ebara M, Aoyagi T: Near-infrared light-responsive shape-memory poly (ϵ-caprolactone) films that actuate in physiological temperature range. *Polymer Journal* 2014, 46:492-498.
77. Naito AT, Shiojima I, Akazawa H, Hidaka K, Morisaki T, Kikuchi A, Komuro I: Developmental stage-specific biphasic roles of Wnt/beta-catenin signaling in cardiomyogenesis and hematopoiesis. *Proc Natl Acad Sci U S A* 2006, 103:19812-19817.
78. D'Souza SE, Ginsberg MH, Plow EF: Arginyl-glycyl-aspartic acid (RGD): a cell adhesion motif. *Trends Biochem Sci* 1991, 16:246-250.
79. Sa S, Wong L, McCloskey KE: Combinatorial fibronectin and laminin signaling promote highly efficient cardiac differentiation of human embryonic stem cells. *Biores Open Access* 2014, 3:150-161.
80. Rangappa S, Entwistle JW, Wechsler AS, Kresh JY: Cardiomyocyte-mediated contact programs human mesenchymal stem cells to express cardiogenic phenotype. *J Thorac Cardiovasc Surg* 2003, 126:124-132.
81. Burridge PW, Matsa E, Shukla P, Lin ZC, Churko JM, Ebert AD, Lan F, Diecke S, Huber B, Mordwinkin NM, et al: Chemically defined generation of human cardiomyocytes. *Nat Methods* 2014, 11:855-860.
82. Uto K, Ebara M, Aoyagi T: Temperature-responsive poly(ε-caprolactone) cell culture platform with dynamically tunable nano-roughness and elasticity for control of myoblast morphology. *Int J Mol Sci* 2014, 15:1511-1524.

83. Woodruff MA, Hutmacher DW: The return of a forgotten polymer—polycaprolactone in the 21st century. *Progress in Polymer Science* 2010, 35:1217-1256.
84. Lendlein A, Langer R: Biodegradable, elastic shape-memory polymers for potential biomedical applications. *Science* 2002, 296:1673-1676.
85. Behl M, Razzaq MY, Lendlein A: Multifunctional shape-memory polymers. *Adv Mater* 2010, 22:3388-3410.
86. Uto K, Yamamoto K, Hirase S, Aoyagi T: Temperature-responsive cross-linked poly(epsilon-caprolactone) membrane that functions near body temperature. *J Control Release* 2006, 110:408-413.
87. Ebara M, Uto K, Idota N, Hoffman JM, Aoyagi T: Rewritable and shape-memory soft matter with dynamically tunable microchannel geometry in a biological temperature range. *Soft Matter* 2013, 9:3074-3080.
88. Ebara M, Uto K, Idota N, Hoffman JM, Aoyagi T: Shape-memory surface with dynamically tunable nano-geometry activated by body heat. *Adv Mater* 2012, 24:273-278.
89. Ebara M, Uto K, Idota N, Hoffman JM, Aoyagi T: The taming of the cell: shape-memory nanopatterns direct cell orientation. *Int J Nanomedicine* 2014, 9 Suppl 1:117-126.
90. Klein I, Danzi S: Thyroid Disease and the Heart. *Curr Probl Cardiol* 2016, 41:65-92.